Diffusion of air molecules in polar ice sheets

Tomoko Ikeda*, Andrey N. Salamatin**, Vladimir Ya. Lipenkov*** and Takeo Hondoh*

*Institute of Low Temperature Science, Hokkaido University, N19W8, Sapporo 060-0819, JAPAN
**Department of Applied Mathematics, Kazan State University, Kazan 420008, RUSSIA
***Arctic and Antarctic Research Institute, St. Petersburg 199397, RUSSIA

Abstract: Ancient atmospheric gases are trapped in polar ice sheets. The gas molecules are stored in air-bubbles at shallower depth. The air-bubbles are gradually compressed with depth and begin to transform into clathrate hydrates below the level at which the hydrostatic pressure becomes greater than the dissociation pressure of the phase of air clathrate hydrate. Air-bubbles and clathrate hydrates coexist in the deep ice over a long period of time. Significant fractionation of gas molecules in the transition zone of Vostok Antarctic ice has been found from measurements of the depth profile of the N_2/O_2 composition ratios in clathrate hydrates and air-bubbles using Raman spectroscopy. In order to understand the fractionation process, a theoretical model of post-nucleation growth of clathrate hydrates caused by the diffusive selective mass transfer of air molecules from air-bubbles through the surrounding ice matrix has been developed. The studies revealed air diffusion between air-bubbles and clathrate hydrates as the principal mechanism of gas fractionation between air-bubbles and clathrate hydrates in deep ice sheets. We review the effect of the transition from air-bubbles to clathrate hydrates on the distribution of air molecules in polar ice sheets.

1. Introduction

Paleoatmospheric reconstruction is one of the main topics of research on ice cores [1–6]. Atmospheric gases are trapped in air-bubbles when firn is transformed into ice by sedimentation near the surface of polar ice sheets. Air-bubbles are compressed with depth and gradually transform into clathrate hydrates below a certain depth [7, 8]. Since the processes of the firn-ice transition and the formation of clathrate hydrates may affect the composition and distribution of the atmospheric gases in ice, these processes have been studied in order to reconstruct accurate records of the paleoatmosphere from polar ice cores [9–21]. In the present review, we focused on the fractionation effect of air molecules during the transition process from air-bubbles to clathrate hydrates in polar ice sheets.

2. Structure of clathrate hydrate in polar ice sheets

Clathrate hydrate is a kind of non-stoichiometric compound, whose composition changes depending on temperature

Physics of Ice Core Records
Edited by T. Hondoh
Hokkaido University Press, 2000, Sapporo

and pressure. Water molecules in clathrate hydrate are linked together by hydrogen bonds in the closest packing of polyhedral cage-like structures that can accommodate a variety of guest molecules. Most clathrate hydrates form one of two distinct crystallographic structures, Stackelberg's structure-I or II [22], depending on the size and shape of the guest molecules.

The crystallographic structure of the host lattice in the structure-I clathrate hydrate was determined by McMullen and Jeffrey [23] from X-ray diffraction study of ethylene oxide clathrate hydrate. A cubic unit cell of dimensions a = 1.203 nm (at 243 K) in space group $Pm3n$ contains 46 water molecules in a framework of two dodecahedral and six tetrakaidecahedral cages. If the cages are fully occupied (i.e., the degree of the site occupancy by guest molecules, y, is equal to unity), the composition of the crystal is $G{\cdot}5.75H_2O$, where G is the guest molecule.

The structure of the host lattice in the structure-II clathrate hydrate was determined by Mak and McMullan [24] from X-ray diffraction study of the double hydrate of tetrahydrofuran and hydrogen sulfide. A cubic unit cell with a dimension a = 1.731 nm (at 253 K) in space group $Fd3m$ contains 136 water molecules in a framework of 16 dodecahedral and eight hexakaidecahedral cages. If the cages are fully occupied (i.e., y = 1), the composition of the crystal is $G{\cdot}5.67H_2O$.

The major guest molecules in natural air clathrate hydrate are N_2 and O_2 (i.e., the major atmospheric gases). Using X-ray and neutron diffraction, Davidson et al. [25, 26] showed that the artificial pure O_2-, pure N_2-, and air- clathrate hydrates form the structure-II. They concluded that very small molecules such as Ar, Kr, N_2, and O_2 form the structure-II, because these molecules are preferentially accommodated in the dodecahedral cages of the structure-II.

Hondoh et al. [27] measured X-ray diffraction of a natural air clathrate hydrate from a depth of 1500 m (i.e., 255.5 K, 13.6 MPa) in the Dye-3 Greenland ice core, and found that the crystallographic structure of the crystal is the structure-II. The lattice constant of the crystal is 1.721 nm at 253 K. From structure refinement analysis, they found that the site occupancies of two cages in the crystal are about 0.8 at 243 K. The guest molecules (i.e., N_2 and O_2) in the dodecahedral cages are located at the centers of the cages and rotate anisotropically about the <111> axis [27, 28]. On the other hand, the guest molecules in the hexakaidecahedral cages are located around the center and rotate isotropically [27, 28]. It was concluded that the crystallographic structure of natural air clathrate hydrates in polar ice sheets is the structure-II [27], because the sizes of the two major guest molecules are sufficiently small to allow the formation of this structure [25, 26].

Kuhs et al. [29] performed neutron powder diffraction work on an artificial N_2 clathrate hydrate over a wide range of pressures. They found that the N_2 clathrate hydrate partially forms the structure-I at pressures exceeding several tens of MPa; that is, the crystallographic structure of the N_2 clathrate hydrate depends on thermodynamic conditions. The phase of the structure-I N_2 clathrate hydrate transforms completely into the structure-II over periods of several weeks to several months, since the structure-I is not thermodynamically stable [29]. The hydrostatic pressures at deeper depth in the polar ice sheets reach several tens of MPa.

However, it is expected that the crystallographic structure of natural air clathrate hydrate at deeper depth in the polar ice sheets will be the structure-II, because the polar ice sheets are maintained for a very long time.

3. Transition process from air-bubbles to clathrate hydrates

Gas molecules are stored in air-bubbles at shallow depth in polar ice sheets. Air-bubbles are compressed with depth and gradually transform into clathrate hydrates below a certain depth, depending on the temperature of the ice sheet [7, 8]. Fig. 1 shows the temperature dependence on the

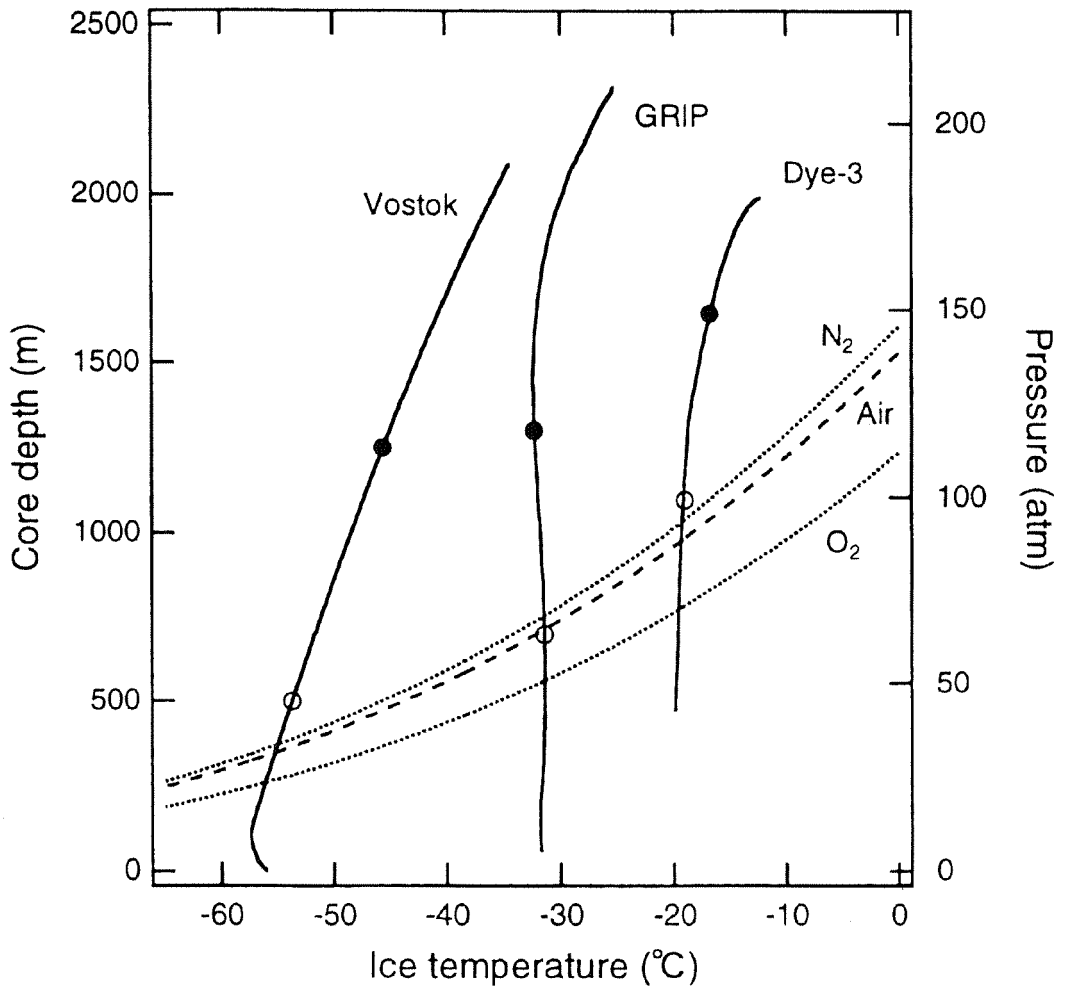

Figure 1: Relationship between temperature and dissociation pressures of N_2-, O_2-, and air- (N_2/O_2 = 3.7) clathrate hydrates. The solid lines are the depth profiles of the ice temperatures of Vostok, GRIP, and Dye-3 ice cores. The open and solid circles show the depths below which clathrate hydrate crystals are observed and below which air-bubbles are not observed, respectively.

formation pressure (i.e., core depth) of clathrate hydrate [7]. The formation of air clathrate hydrate starts when pressure is equal to the dissociation pressure P^d, which is a function of the composition of the gas mixture and the temperature. P^d is given by

$$P^d = \frac{P^d{}_{N2} P^d{}_{O2}}{Z_{N2} P^d{}_{O2} + Z_{O2} P^d{}_{N2}} , \qquad (1)$$

where $P^d{}_{N2}$ and $P^d{}_{O2}$ are the respective dissociation pressures of pure N_2- and O_2-clathrate hydrates, and Z_{N2} and Z_{O2} are the mole fractions of N_2 and O_2 in the gas phase, respectively [30]. $P^d{}_{N2}$ and $P^d{}_{O2}$ (MPa) at the temperature T (K) are given by [7]

$$\log P^d{}_{N2} = 3.6905 - 688.9/T ,$$
$$\log P^d{}_{O2} = 3.679 - 717/T . \qquad (2)$$

Clathrate hydrates and air-bubbles coexist in a deep ice sheet within a range of depth (the transition zone), as shown in Fig. 2. For instance, the transition zone in the Vostok Antarctic ice is 500–1250 m in depth [31, 32] (see Fig. 1), which corresponds to a time period of about 35 kyr [20]. The transition times for the Dye-3 and the GRIP Greenland ice cores are about 4.1 kyr [33] and 4.5 kyr [34], respectively. Several studies have been carried out to clarify why air-bubbles and clathrate hydrate crystals coexist in deep ice sheets over such a long period of time.

Using a high-pressure cell on an optical microscope stage, Uchida et al. [35, 36] observed the formation and growth processes of air clathrate hydrate crystals on the walls of air-bubbles (i.e., on ice crystals). They distinguished the growth

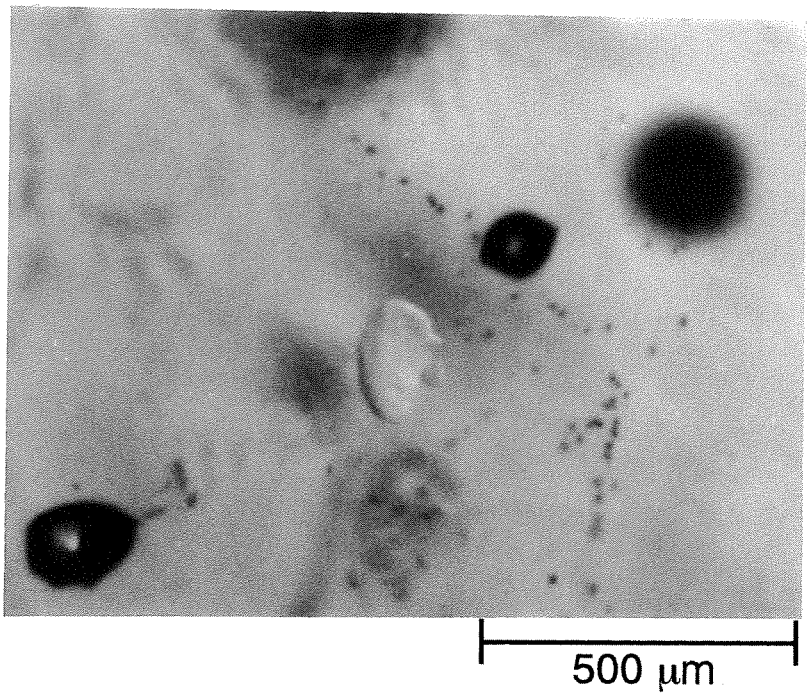

Figure 2: Clathrate hydrate and air-bubbles at a depth of 750 m within the transition zone in the Vostok Antarctic ice core. The object at the center is the clathrate hydrate crystal.

process of a clathrate hydrate crystal after nucleation into the following two stages: (1) surface coating of the wall of the air-bubble by the clathrate hydrate, and (2) growth as a shell of clathrate hydrate, filling up the air-bubble. From observation of the growth rate of clathrate hydrate, they estimated the activation energies for these two growth stages to be 50 and 87 $kJ \cdot mol^{-1}$, respectively. They concluded that the first growth stage is mainly controlled by the diffusion of water molecules through the ice lattice toward the wall of the air-bubble, because the activation energy was similar to that for self-diffusion of water molecules in ice Ih [37]. The larger activation energy for the second growth stage was applied to the diffusion of air and water molecules through the shell of the clathrate hydrate in opposite directions. Based on the growth rate of the clathrate hydrate, they showed that the time period of the transformation of an air-bubble into a clathrate hydrate in a deep ice sheet is significantly shorter than the time period of the transition zone. Thus, they concluded that a very long time period of the transition zone is attributed to the difficulty of nucleation of the clathrate hydrate on the wall of the air-bubble.

On the other hand, Price [38] proposed a growth-limited mechanism to explain the very long time period of the transition zone. Disregarding the stage of nucleation, he used a water-diffusion model to interpret the distribution of the number concentrations of air-bubbles and clathrate hydrates in the transition zone in the Vostok and the Byrd ice cores [31, 32, 39, 40]. As a result, he estimated that the diffusion coefficient of water molecules in clathrate hydrate is several orders of magnitude smaller than that in ice. Thus, he concluded that the post-nucleation growth of clathrate hydrate takes the whole time period covered by the transition zone.

However, Hondoh [41] pointed out that some air-bubbles are completely transformed to clathrate hydrate already at the beginning of the transition zone and that air-bubbles free from the formation of clathrate hydrate still exist at the end of the zone in the Vostok ice cores. This means that the post-nucleation growth is very rapid compared to the time period of the transition zone. In addition, he estimated that the diffusion coefficient of water molecules in clathrate hydrate is about three orders of magnitude larger than that in ice.

The patterns of the growth process of clathrate hydrate were classified into two types A and B from optical microscopic observations of secondary growth of clathrate hydrate in air cavities formed due to the decomposition of the initial clathrate hydrate crystals after ice core recovery (See Fig. 3) [35]. Salamatin et al. [30] modeled the growth process of type A, in which the clathrate hydrate crystal, after nucleation, rapidly coats the wall of the air-bubble and then grows as a spherical hydrate shell, filling up the air-bubble. According to their theoretical model, a considerable amount of air molecules (30–70 % of the total mass) in the air-bubble is abruptly converted to the clathrate hydrate crystal after nucleation because of the high supersaturation of the initial air-bubble. The amount of air molecules, which convert to the clathrate hydrate at this initial stage, depends on the depth of the nucleation (i.e., the degree of the supersaturation in the initial air-bubble). This initial stage of the transformation is rather short and takes about one month under the conditions in the Vostok ice. During this stage, the pressure of the air-bubble simultaneously drops to the

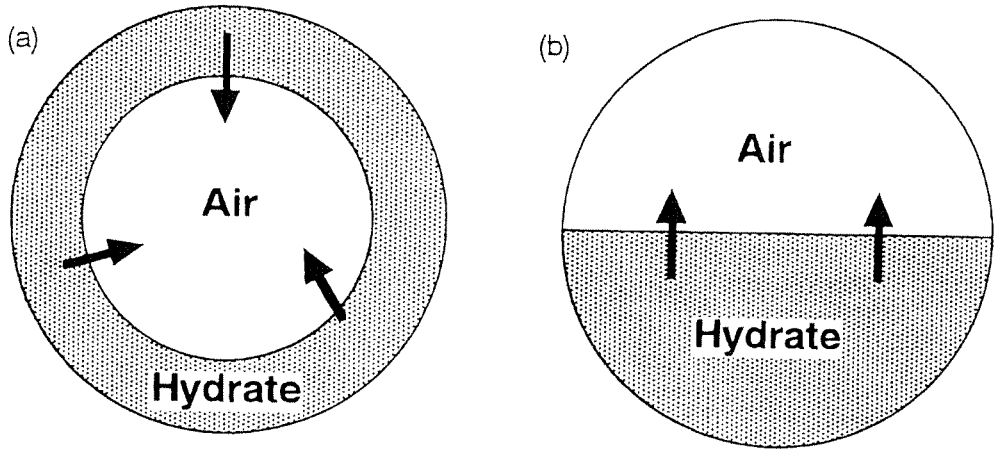

Figure 3: Two types of growth process of clathrate hydrate from an air-bubble. (a) Type A. The clathrate hydrate crystal, after nucleation, rapidly coats the wall of the air-bubble and then grows as a spherical hydrate shell, filling up the air-bubble. (b) Type B. The clathrate hydrate crystal does not coat the whole wall of the air-bubble but gradually grows inward, maintaining a flat interface with the gas phase.

dissociation pressure level. Then, the shell of the clathrate hydrate grows, filling up the air-bubble. These growth occurs due to 1) diffusion of air and water molecules through the clathrate hydrate layer in opposite directions, and 2) hydrostatic compression of the air-bubble confined to the shell of the clathrate hydrate and surrounding ice, both plastically deformed under the excess load pressure. They concluded that the compression of the air-bubble is the rate-limiting step in post-nucleation growth of the clathrate hydrate and that the typical time of this growth process is about 100 yr in the middle of the transition zone of the Vostok ice cores.

Furthermore, Salamatin et al. [20] modeled the growth process of type B, in which the clathrate hydrate crystal does not coat the whole wall of the air-bubble but gradually grows inward, maintaining a flat interface with the gas phase. According to their theoretical model, a considerable amount of air molecules in the air-bubble is abruptly converted to the clathrate hydrate crystal after nucleation, as is the case for type A. They showed that the typical time of compression of the air-bubble in the growth process of type B can be one order of magnitude shorter than that in type A, because the absence of the hard shell of clathrate hydrate around the air-bubble reduces the compression time. For both types of growth process, the time scale of the post-nucleation transformation from an air-bubble to a clathrate hydrate in the polar ice sheets is at least 2–4 orders of magnitude shorter than the duration of the transition. Therefore, it was concluded that the very long time period of the transition zone (e.g., on the order of 10^4 years in the Vostok ice cores) is due to the extremely low probability of nucleation of the clathrate hydrate. This conclusion was later

supported by the results of the measurements of the depth profiles of N_2/O_2 composition ratios in clathrate hydrates and air-bubbles using Raman spectroscopy [19].

4. General aspects of gas fractionation during the transition process

4.1. Compositions of air molecules in clathrate hydrates and air-bubbles

When clathrate hydrate is formed in a ternary system (i.e., a gas mixture and H_2O), the gases are fractionated by selective enclathration [42, 43]. Von Stackelberg [44] found that the air liberated from chloroform clathrate hydrate prepared in the presence of air is much enriched in O_2. Thus, fractionation of air gases in natural air clathrate hydrate is expected. Several studies have been carried out to investigate the effect of fractionation during the transition process from air-bubbles to clathrate hydrates in polar ice sheets [11, 14–19].

Raman spectroscopy allows excitation of intramolecular vibration modes of the gas molecules contained in the clathrate hydrates with no influence from the ice matrix. Nakahara et al. [11] measured Raman spectra of clathrate hydrates from a depth of 1501 m in the Dye-3 ice core. Since the frequencies of two peaks at 2322 and 1546 cm^{-1} in the observed spectra were close to those of the stretching modes of N_2 and O_2 gases, they identified the major guest molecules in the clathrate hydrate as N_2 and O_2. From the scattering intensities of the peaks of N_2 and O_2, they found that the N_2/O_2 composition ratio averaged over three clathrate hydrate crystals was 1.7. Atmospheric gas was used as a standard to estimate the N_2/O_2 composition ratio from the N_2/O_2 peak intensities ratio. The value in their study (1.7) is much smaller than the present atmospheric ratio of 3.7. They concluded that this enrichment of O_2 was due to the lower dissociation pressure for pure O_2 clathrate hydrate than that for pure N_2 clathrate hydrate.

In contrast, Pauer et al. [14, 18] showed there was no significant enrichment of gases in clathrate hydrates from measurements of Raman spectra of 144 clathrate hydrates from different depths between 1219 and 2923 m in the GRIP ice cores. The N_2/O_2 ratio averaged over 144 clathrate hydrates was 3.6, which was close to the atmospheric ratio. They claimed that the enrichment of O_2 found in the Dye-3 ice cores [11] must be due to a relaxation-induced change after coring. They predicted that the difference in the dissociation pressures between pure N_2- and O_2-clathrate hydrates causes the distribution of N_2/O_2 ratios within an individual clathrate hydrate crystal.

In order to investigate the fractionation effect on an individual clathrate hydrate crystal, Pauer et al. [15] measured the focal plane dependence of the N_2/O_2 ratio within a clathrate hydrate from a depth of 1475.65 m in the GRIP ice core using Raman spectroscopy. However, they found no fractionation effect (i.e., gradient) on the N_2/O_2 concentration within the clathrate hydrate crystal, which is in contrast to the different dissociation pressures for pure N_2- and O_2- clathrate hydrates. They concluded that the gradient of the concentration resulted from the initial fractionation may have been leveled out with time.

On the other hand, Fukazawa et al. [16] measured the Raman spectra of both clathrate hydrates and air-bubbles in the beginning of the transition zone of the

Vostok ice cores (650 and 750 m in depth). They found that the N_2/O_2 ratios in the clathrate hydrates were very low (1.0–2.5), while those in the air-bubbles were close to the atmospheric ratio. They proposed that clathrate hydrates at the beginning of the transition zone are enriched in O_2.

In order to clarify the mechanism of fractionation during the transition process from air-bubbles to clathrate hydrates, Ikeda et al. [19] investigated the depth profile of the N_2/O_2 ratios in both air-bubbles and clathrate hydrates over a wide range of depths in the Vostok ice cores. They measured Raman spectra of 140 clathrate hydrates and 120 air-bubbles from depths between 83 to 3316 m in the Vostok ice cores. This depth range includes all three zones, that is, the bubbly ice (pre-transition) zone, the transition zone, and the bubble-free ice (post-transition) zone. The Raman spectra of O_2- and N_2- stretching vibration modes for a clathrate hydrate and an air-bubble are shown in Fig. 4. The composition ratio of N_2 and O_2 was assumed to be equal to the ratio of their Raman peak intensities. As a result, they found the remarkable variations of the N_2/O_2 ratios in clathrate hydrates and air-bubbles with depth presented in Fig. 5.

Fig. 5 shows depth profiles of the N_2/O_2 ratios of air-bubbles and of clathrate hydrates [19]. Each data point represents the average N_2/O_2 ratio for about 6 air-bubbles or 6 clathrate hydrates. As indicated by the standard deviations in the figure, the N_2/O_2 ratios are widely distributed, depending on the individual

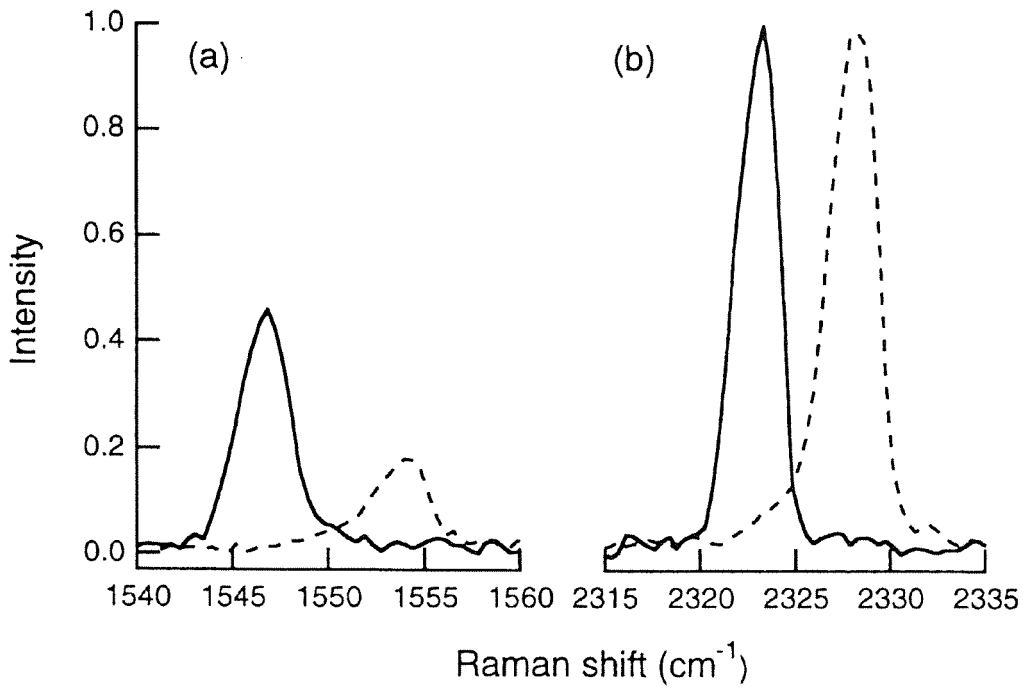

Figure 4: Raman spectra of (a) O_2- and (b) N_2- stretching vibration modes for a clathrate hydrate and an air-bubble in the Vostok ice core (750 m in depth). The solid and broken lines show the spectra of a clathrate hydrate and an air-bubble, respectively.

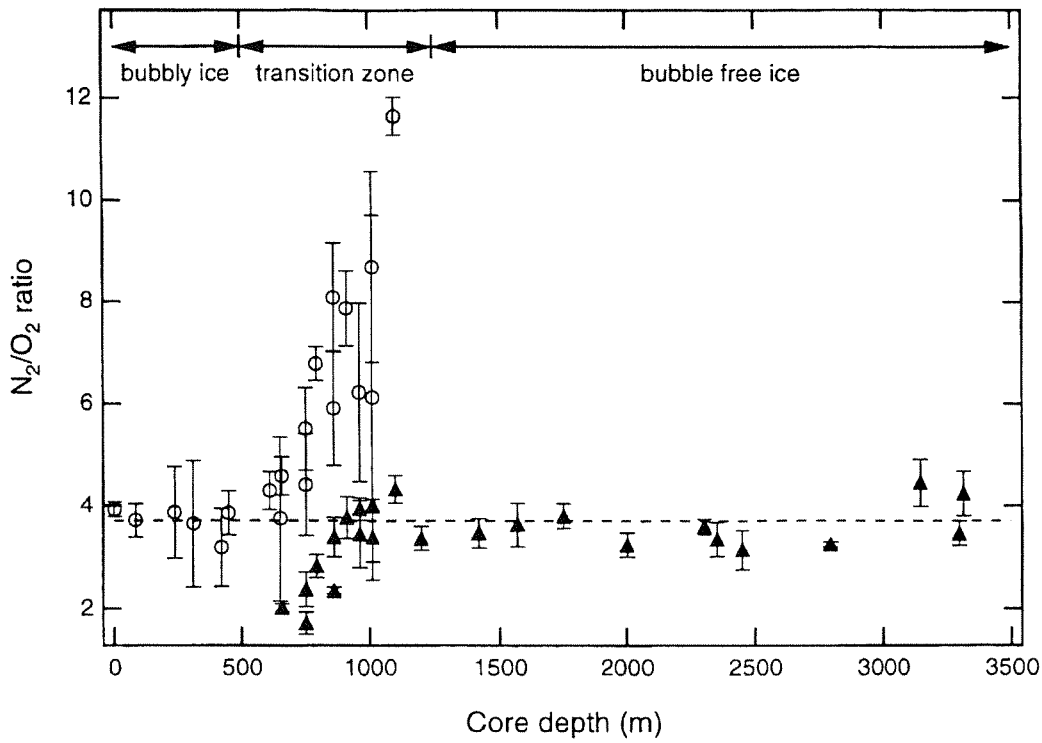

Figure 5: Depth profiles of N_2/O_2 ratios of clathrate hydrates and of air-bubbles [19]. The solid triangles and the open circles are the average values for clathrate hydrates and air-bubbles, respectively. The error bars attached are the standard deviations for scattering of the data at the same depth. The broken horizontal line shows the value of the atmospheric ratio (3.7).

species. In the transition zone, however, a great systematic change in the average values can be seen. For air-bubbles, the average N_2/O_2 ratios increase from the atmospheric ratio of 3.7 at the beginning of the transition zone to 11.7 at the end. In contrast, N_2/O_2 ratios of clathrate hydrates are significantly smaller than the atmospheric ratio at the beginning of the transition zone and approach the atmospheric ratio with increases in depth. The average N_2/O_2 ratio of clathrate hydrates is 2.0 at the beginning and 3.6 at the end of the transition zone. The N_2/O_2 ratio of the total gas content in the clathrate hydrates and the air-bubbles in the transition zone is estimated to be 3.9 using the data of volume concentrations of clathrate hydrates and air-bubbles [45]. In the other two zones, no systematic change in the N_2/O_2 ratio was found. The N_2/O_2 ratios averaged over the air-bubbles in the bubbly ice zone and averaged over the clathrate hydrates in the bubble-free ice zone are 3.7 and 3.6, respectively.

4.2. Fractionation process of air molecules

The variations of the N_2/O_2 ratios in the clathrate hydrates and the air-bubbles with depth in the transition zone of the Vostok ice cores could be caused by one of

the following possible mechanisms: (1) relaxation-induced change after coring, (2) thermodynamic fractionation caused by the difference in the dissociation pressures between pure N_2- and O_2- clathrate hydrates, and (3) diffusive mass transfer of air molecules between clathrate hydrates and air-bubbles through the ice matrix. The mechanism (1) can be ruled out, because the temperature of the ice cores was kept below −50 °C after coring. The degree of the site occupancy of clathrate hydrate in equilibrium with the ice and air phases is determined by dissociation pressure (i.e., temperature) [46]. Thus, the variation in the composition of gas molecules in clathrate hydrate with decrease in pressure due to core relaxation is negligibly small [47].

The mechanism (2) can also be ruled out by the following reason. If an initially formed small clathrate hydrate crystal is separated from the remaining air-bubble, the clathrate hydrate is enriched in oxygen. The composition of the clathrate hydrate can be estimated using the solid-solution model [46]. This model is a thermodynamic model in which the guest molecules are dissolved or absorbed in the host lattice. Under the assumption of equal site occupancy for pure N_2- and O_2- clathrate hydrates at the dissociation pressures, based on the model [46], the N_2/O_2 ratio in a clathrate hydrate transformed from a gas mixture of N_2 and O_2 is given by

$$Y_{N2}/Y_{O2} = P^d{}_{O2} Z_{N2} / Z_{O2} P^d{}_{N2} \ , \qquad (3)$$

where Y_{N2} and Y_{O2} are the mole fractions of N_2 and O_2 in the clathrate hydrate, respectively. At the beginning of the transition zone in the Vostok ice (i.e., at 220 K), $P^d{}_{N2}$ and $P^d{}_{O2}$ are 3.6 and 2.6 MPa, respectively, using Eq. (2). When the N_2/O_2 ratio in the initial air-bubble (i.e., Z_{N2}/Z_{O2}) was 3.7, the minimum value of the N_2/O_2 ratio (i.e., Y_{N2}/Y_{O2}) in the clathrate hydrate transformed from the air-bubble is 2.7. This value is significantly larger than the smallest value observed by Ikeda et al. [19] (i.e., 1.5). In addition, the probability of separation of the clathrate hydrate from the remaining air-bubble at the beginning of the transition zone seems to be very low, according to the results of optical microscopic observations of number concentrations of air-bubbles and clathrate hydrates in the Vostok ice cores [45].

In most cases, one air-bubble is transformed into one clathrate hydrate crystal [45]. Thus, the N_2/O_2 ratio of the total gas molecules in the clathrate hydrate crystal is equal to the value of the original air-bubble, if there is no mass transfer of gas through the surrounding ice matrix. However, the N_2/O_2 ratios in clathrate hydrates and air-bubbles change with depth [19]. From the data of total gas contents and volume concentrations of air-bubbles and clathrate hydrates in the Vostok ice cores, it has been confirmed that the amount of gases dissolved in ice crystal is very small in comparison with the total amount of gases included in both clathrate hydrates and air-bubbles [45]. Therefore, it was concluded that the variation in the N_2/O_2 ratios in clathrate hydrates and air-bubbles in the transition zone is caused by the diffusive mass transfer of air molecules between clathrate hydrates and air-bubbles through the ice matrix (i.e., the mechanism (3)).

4.3. Diffusion of air molecules in ice

The diffusion of air molecules in polar ice cores is thought to be driven by a

gradient of the concentration of air molecules dissolved in ice between clathrate hydrates and air-bubbles [19]. This gradient exists due to the high pressure in air-bubble in comparison with the approximately constant dissociation pressure of clathrate hydrate in the transition zone.

The concentrations of N_2 and O_2 molecules in ice including both air-bubbles and clathrate hydrates coexist are estimated as follows. The concentration of gas molecules dissolved in the lattice of the ice Ih, C, depends on the size and shape of the gas molecules. Fig. 6 shows the relationship between the fractional concentration (at 263 K, 1 MPa) and van der Waals radius for various gas molecules [41]. By extrapolating the line to the radii of N_2 and O_2, the concentrations of N_2 and O_2 dissolved in ice, C_{N2} and C_{O2}, are estimated to be 1.8×10^{-7} and 2.6×10^{-7} $mol \cdot mol_{H2O}^{-1} \cdot MPa^{-1}$ (at 263 K, 1 MPa), respectively. Under the assumption that the concentrations vary little with variation in temperature [41, 48], we attempted to apply these estimations to the conditions in polar ice sheets.

When a block of ice includes only air-bubbles, the equilibrium concentrations of N_2 and O_2 dissolved in ice, X_{N2}^{B} and X_{O2}^{B}, are proportional to the partial pressures of N_2 and O_2 in the air-bubbles, as shown in Fig. 7. After nucleation of a clathrate hydrate, the equilibrium concentrations of N_2 and O_2 in ice at the interface with the clathrate hydrate, X_{N2}^{H} and X_{O2}^{H}, are proportional to the degree of site occupancy by air in the clathrate hydrate (i.e., y).

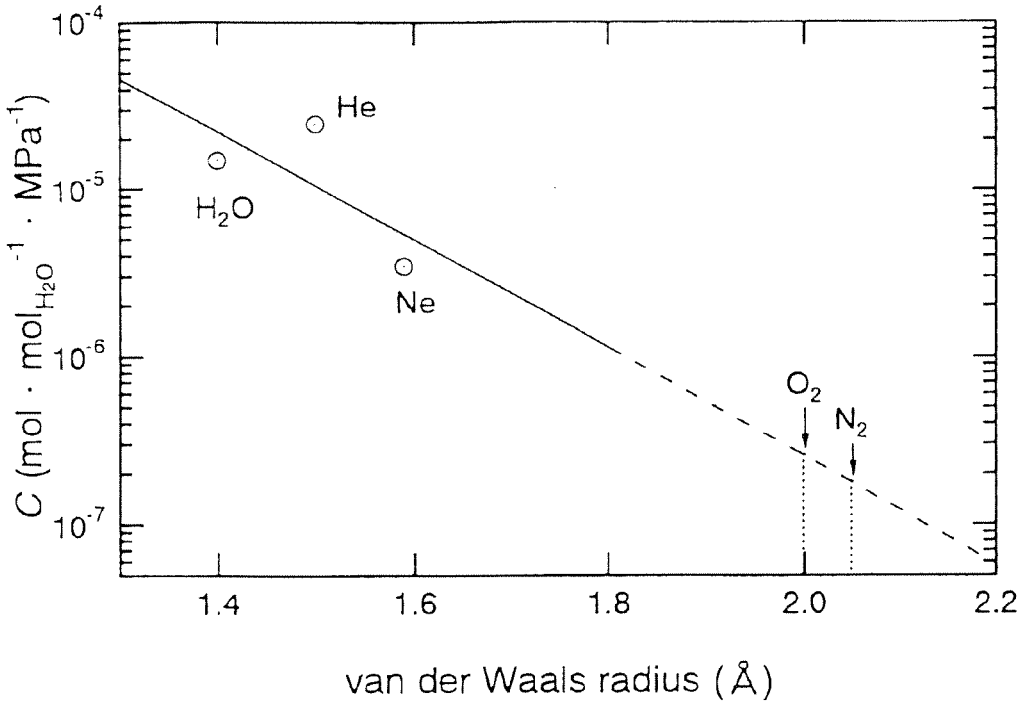

Figure 6: Relationship between the fractional concentrations C (at 263 K, 1 MPa) and van der Waals radii [41]. The data of C are from the literature: H_2O, He, and Ne [37, 48].

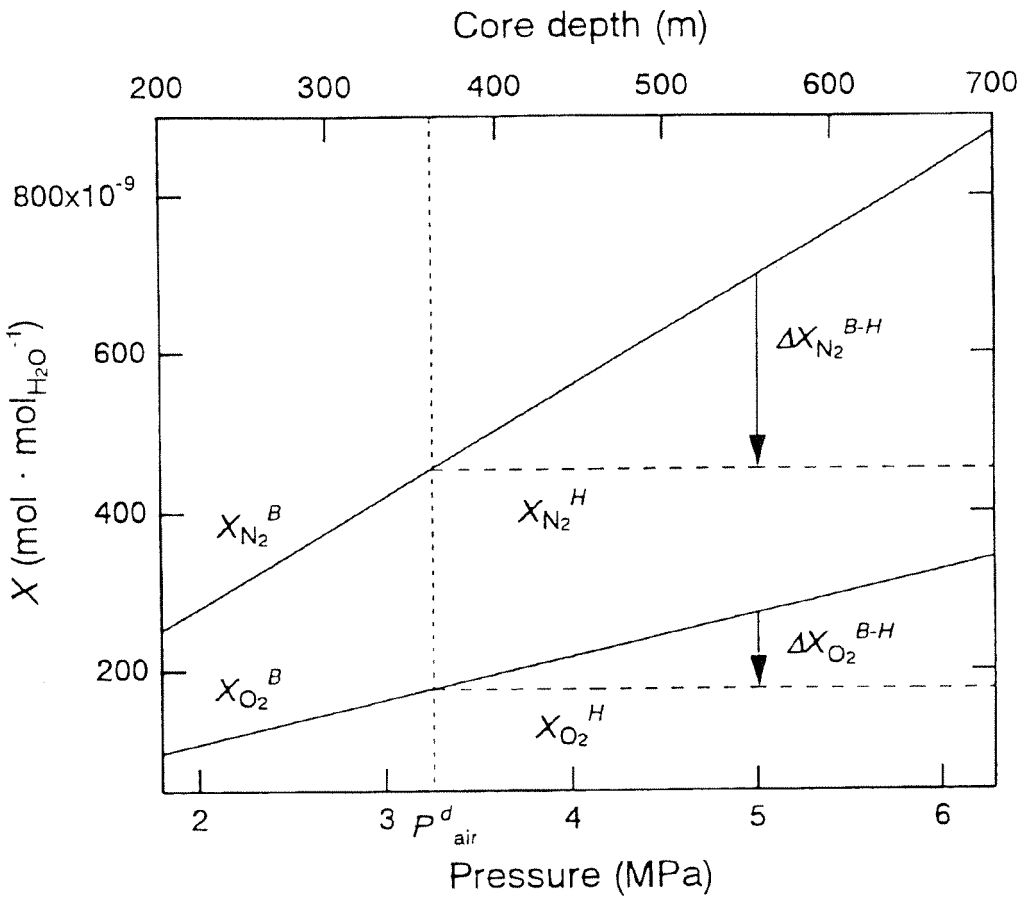

Figure 7: Concentrations of N_2 and O_2 dissolved in ice. X_{N2}^{B} and X_{O2}^{B} are the equilibrium concentrations of N_2 and O_2 dissolved in ice at the interface with air-bubble, respectively. X_{N2}^{H} and X_{O2}^{H} are the equilibrium concentrations of N_2 and O_2 dissolved in ice at the interface with clathrate hydrate, respectively. ΔX_{N2}^{B-H} and ΔX_{O2}^{B-H} are the concentration differences of N_2 and O_2 in ice between the air-bubbles and the clathrate hydrates, respectively. The N_2/O_2 ratios of the clathrate hydrate and the air-bubble are 3.7.

Because of the equilibrium of three phases (i.e., ice including air, clathrate hydrate, and air in air-bubble), X_{N2}^{H} (or X_{O2}^{H}) is equal to X_{N2}^{B} (or X_{O2}^{B}) at the dissociation pressure of the air clathrate hydrate P^d. Since the variation of y with temperature along the transition zone is negligibly small, it can be assumed that the values of X_{N2}^{H} and X_{O2}^{H} are constant, as shown in Fig. 7. Therefore, diffusive fluxes of N_2 and O_2 are driven by the concentration differences of N_2 and O_2 in ice between the air-bubbles and the clathrate hydrates, ΔX_{N2}^{B-H} and ΔX_{O2}^{B-H}, respectively.

The N_2/O_2 ratios in air-bubbles and clathrate hydrates vary with time because of the difference in the diffusion rates between N_2 and O_2. Since the diffusion coefficients D of N_2 and O_2 in ice, D_{N2} and D_{O2}, are too small to measure directly, no experimental

data on the values of D_{N2} and D_{O2} have previously been reported. Thus, using the relationship between the values of D and the van der Waals diameters of various gas molecules, Satoh et al. [48] roughly estimated the diffusion coefficients of N_2 and O_2, D_{N2} and D_{O2}, to be 1.4×10^{-12} and 8.7×10^{-13} $m^2 \cdot s^{-1}$ (at 263 K, 0.1 MPa), respectively. However, they used the inappropriate values of 0.41 and 0.42 nm as the largest van der Waals diameters of N_2 and O_2, respectively. With the correct largest van der Waals diameters (i.e., 0.41 and 0.40 nm), the values of D_{N2} and D_{O2} are recalculated to be 1.4×10^{-12} and 2.2×10^{-12} $m^2 \cdot s^{-1}$, respectively. In addition, taking into account the mechanism of diffusion, an alternative method can be used to estimate the value of D.

An interstitial mechanism, similar to that of self-diffusion in ice [37], can be assumed for diffusion of small gas molecules; i.e., a gas molecule migrates by jumping from a stable interstitial site to an adjacent site through a narrow space in the lattice. There are two crystallographically non-equivalent interstitial sites designated Tu (uncapped trigonal) and Tc (capped trigonal) in ice Ih, as shown in Fig. 8. The jumping rate at the temperature T is

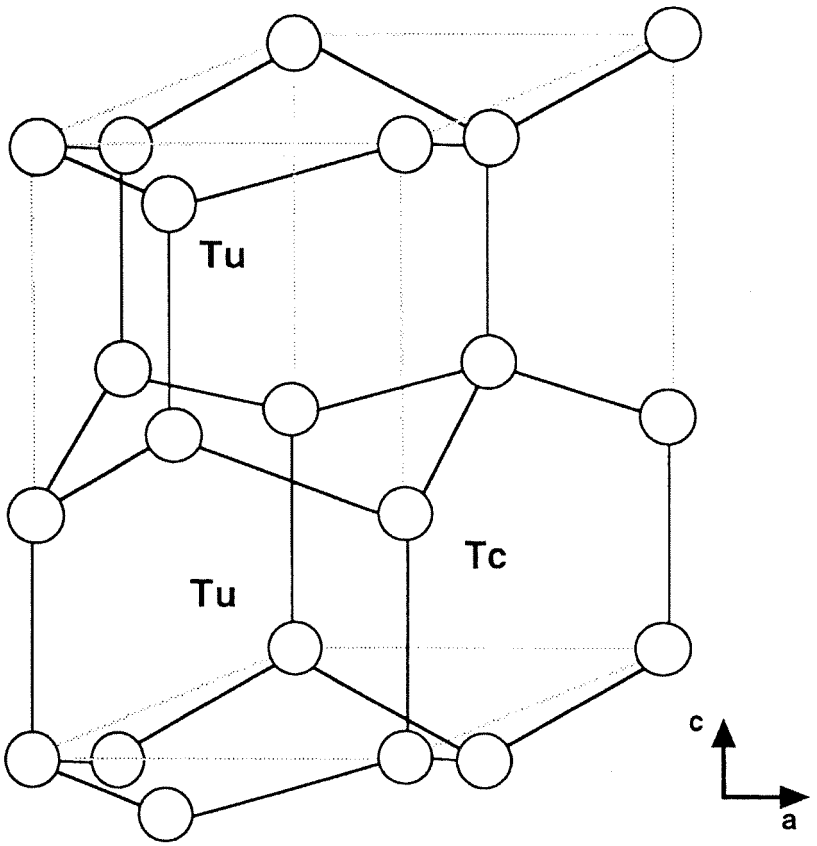

Figure 8: Crystallographic structure of ice Ih. The open circles are the sites of oxygen atoms. Two kinds of interstitial site are described as Tu (uncapped trigonal) and Tc (capped trigonal).

proportional to $\exp(-Q/kT)$, where Q is the activation energy for the jump, and k is the Boltzmann constant. The potential barrier ΔE can be used as a measure of Q. The value of ΔE is calculated from the intermolecular interaction energies between a gas molecule and surrounding water molecules.

The intermolecular interaction energy is taken as the sum of a repulsion-dispersion term and an electrostatic term. For the repulsion-dispersion term $E_{r\text{-}d}$, the Lennard-Jones potential is used:

$$E_{r-d}(r_{wm}) = 4\varepsilon_{wm}\left[\left(\frac{\sigma_{wm}}{r_{wm}}\right)^{12} - \left(\frac{\sigma_{wm}}{r_{wm}}\right)^{6}\right], \tag{4}$$

where r_{wm} is the distance between a water molecule and a gas molecule, ε_{wm} is the potential minimum that corresponds to a separation of $r_{wm} = 2^{1/6}\sigma_{wm}$, and σ_{wm} is the separation at which the attractive and repulsive energies are equal. The values of ε_{wm} and σ_{wm} for the interaction energies between a water molecule and a gas molecule are given by

$$\varepsilon_{wm} = (\varepsilon_w \varepsilon_m)^{1/2},$$
$$\sigma_{wm} = (\sigma_w + \sigma_m)/2, \tag{5}$$

where ε_w, ε_m, σ_w, and σ_m are the empirical intermolecular parameters for water and gas molecules, determined from independent measurements made in the gas phase; the data used include the virial coefficients and the viscosity [43, 49, 50]. The electrostatic term E_e is estimated using the following classical coulombic type interaction:

$$E_e(r_{ij}) = \frac{1}{4\pi\varepsilon_0}\sum_{ij}\frac{q_i q_j}{r_{ij}}, \tag{6}$$

where r_{ij} is the interatomic distance, and q_i and q_j are the charges for individual atoms [51, 52]. Figs. 9(a) and (b) show the intermolecular interaction energies between a gas molecule and surrounding water molecules, $E_{//}$ and $E_{\perp}$, when the gas molecule jumps parallel to the c-axis (i.e., Tu→ Tu) and when the gas molecule jumps perpendicularly to the c-axis (i.e., Tu→ Tc→ Tu), respectively.

The potential barriers for jumps parallel and perpendicular to the c-axis, $\Delta E_{//}$ and $\Delta E_{\perp}$, are taken as the differences between the maximum and minimum values for $E_{//}$ and $E_{\perp}$, respectively. Under the assumption that the probability of a jump parallel to the c-axis is equal to that perpendicular to the c-axis, the averaged diffusion coefficient D is $(D_{//}+D_{\perp})/2$, where $D_{//}$ and $D_{\perp}$ are the diffusion coefficients for the diffusions parallel and perpendicular to the c-axis, respectively. Thus, the averaged potential barrier ΔE is given by

$$\Delta E = -kT\ln\left[\frac{1}{2}\left\{\exp\left(-\frac{\Delta E_{//}}{kT}\right) + \exp\left(-\frac{\Delta E_{\perp}}{kT}\right)\right\}\right]. \tag{7}$$

The values of ΔE for N_2, O_2, H_2O, H, He, Ne, and Ar were calculated using Eq. (7). Fig. 10 shows the relationship between D and ΔE for these molecules [19]. The data of D for H_2O, H, He, Ne, and Ar are from the literatures [37, 48, 53]. By extrapolating the line to larger values of ΔE for N_2 and O_2, D_{N2} and D_{O2} are estimated to be 1.6×10^{-13}

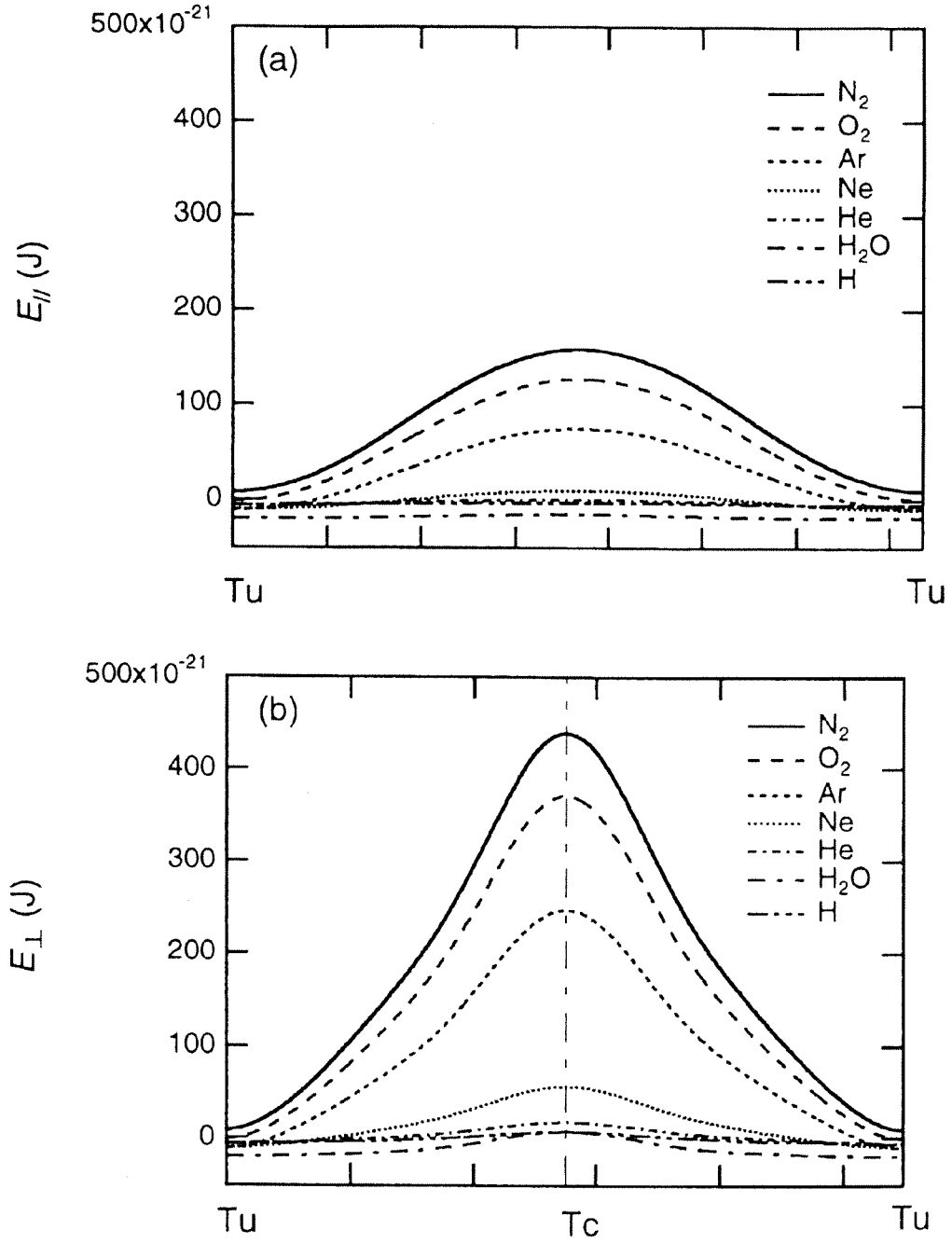

Figure 9: The intermolecular interaction energies between a gas molecule and surrounding water molecules. (a) The gas molecules jump in ice Ih parallel to the c-axis (i.e., Tu→ Tu). (b) The gas molecules jump in ice Ih perpendicular to the c-axis (i.e., Tu→ Tc→ Tu).

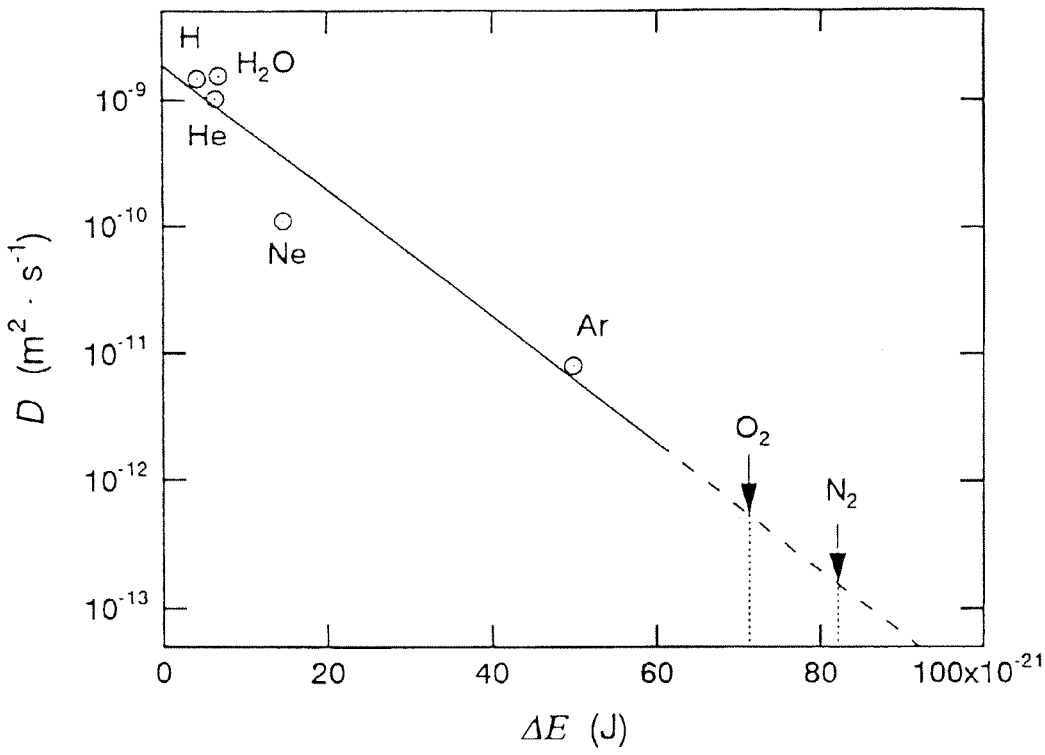

Figure 10: Relationship between the diffusion coefficient D (at 263 K, 1 atm) and the potential barrier parameters ΔE for various gas molecules [19]. The data of ΔE are calculated using Eq. (7). The data of D for H_2O, H, He, Ne, and Ar are from the literatures [37, 48, 53].

and 5.5×10^{-13} $m^2 \cdot s^{-1}$ (at 263 K, 0.1 MPa), respectively [19]. These values are about one order smaller than the above estimates based on the van der Waals diameters (i.e., 1.4×10^{-12} and 2.2×10^{-12} $m^2 \cdot s^{-1}$, respectively), although the tendency of $D_{N2} < D_{O2}$ is consistent. We suppose that the difference between the two estimates is caused by the uncertainty of the estimates based on the van der Waals diameters. It is concluded that the variation in N_2/O_2 ratios of air-bubbles and of clathrate hydrates is attributed to the faster diffusion of O_2 in comparison with N_2 in the ice lattice.

This conclusion is consistent with the results of optical microscopic observations of the sizes of air-bubbles and clathrate hydrates in the Vostok ice cores [45]. The average diameter of very small air-bubbles (i.e., micro-bubbles [45]) is about 0.05 mm at the beginning of the transition zone in the Vostok ice (i.e., at 220 K, 5.1 MPa). Micro-bubbles seem to be preferentially transformed to clathrate hydrates at the beginning of the transition zone. Under the assumption that the lattice constant and the degree of site occupancy of the clathrate hydrate are 1.721 nm and 0.8, respectively [27], the diameter of the clathrate hydrate transformed from a micro-bubble of 0.05 mm in diameter is about 0.04 mm. However, the average diameter of clathrate hydrates at the beginning of the transition zone in the Vostok ice is about 0.06 mm. This result

indicates the post-nucleation growth of clathrate hydrate crystal, which is caused by the diffusion of air molecules from the surrounding air-bubbles through the ice matrix.

The coexistence of air-bubbles and clathrate hydrates is responsible for the fractionation of the concentrations of gases found in the Vostok ice cores. This conclusion is consistent with the theory that nucleation is the rate-limiting process of the transition, as described in section 3 [19].

4.4. Model of the hydrate crystal growth caused by diffusion of air molecules in ice

On the basis of previous theoretical studies [30], Salamatin et al. [20] developed a mathematical model of the post-nucleation growth of clathrate hydrate caused by the diffusive selective mass transfer of air molecules from air-bubbles through the surrounding ice matrix. Using this model, they performed simulations of the two types of the growth process (i.e., the types A and B) of the clathrate hydrates in the transition zone of the Vostok ice cores. They showed that the hydrostatic compression of air-bubbles is the rate-limiting step of the phase transformation, which is influenced by selective diffusion of air molecules.

To evaluate the diffusive mass fluxes, they used the conventional cell-model approximation for diluted multiphase media. A spherical semibubble with growing clathrate hydrate with the external radius r_h is confined to a spherical ice cell of a specific volume related to one inclusion. That is, the radius of the ice cell is given by $r_c = (4\pi N_0/3)^{-1/3}$, where N_0 is the number concentration of all inclusions (i.e., clathrate hydrates and air-bubbles). The N_2 and O_2 molecules diffuse through the spherical ice layer toward its center occupied by the semibubble with growing clathrate hydrate.

The averaged N_2 and O_2 mass fluxes through the ice layer toward the semibubble with growing clathrate hydrate are given by

$$q_{N_2} = 4\pi D^s{}_{N_2}\left[\gamma\frac{P_l}{P^d{}_{N_2}}\overline{Z}_{N_2} + (1-\gamma)\overline{Y}_{N_2} - Y_{N_2}\right]\frac{r_c r_h}{r_c - r_h},$$

$$q_{O_2} = 4\pi D^s{}_{O_2}\frac{M_{N_2}}{M_{O_2}}\left[\gamma\frac{P_l}{P^d{}_{O_2}}\overline{Z}_{O_2} + (1-\gamma)\overline{Y}_{O_2} - Y_{O_2}\right]\frac{r_c r_h}{r_c - r_h}, \quad (8)$$

where $D^s{}_{N2}$ and $D^s{}_{O2}$ are the diffusive permeation (self-diffusion) coefficients of N_2 and O_2, respectively, at a given temperature and dissociation pressure [20]. Y_{N2} and Y_{O2} are the mole fractions of N_2 and O_2 of clathrate hydrate growing on the wall of an air-bubble, respectively. $\overline{Z}_{N_2}$ and $\overline{Z}_{O_2}$ are the mean mole fractions of N_2 and O_2 of surrounding non-nucleated air-bubbles, and $\overline{Y}_{N_2}$ and $\overline{Y}_{O_2}$ are the mean mole fractions of N_2 and O_2 of surrounding completely formed clathrate hydrates. P_l is the load pressure. M_{N2} and M_{O2} are the mole masses of N_2 and O_2, respectively. γ is the averaging parameter, which ranges from 0 to 1 and is assumed to be equal to the number fraction of non-nucleated air-bubbles n_b in N_0.

By constraining the model to the experimental results [19], Salamatin et al. [20] estimated the values of $D^s{}_{N2}$ and $D^s{}_{O2}$ at the beginning of the transition zone in the Vostok ice core (i.e., at T = 220 K, $P^d{}_{N2}$ =

3.6 MPa, and P^d_{O2} = 2.6 MPa) to be 1.4 × 10^{-21} and 3.0 × 10^{-21} $m^2 \cdot mol \cdot mol_{H2O}^{-1} \cdot s^{-1}$, respectively. The diffusive permeation coefficient D^s in ice is given by [37]

$$D^s = XD \ . \tag{9}$$

Using the estimates of X and D (based on ΔE) described in the previous section, D^s_{N2} and D^s_{O2} at 263 K (i.e., at P^d_{N2} = 11.8 MPa, and P^d_{O2} = 9.0 MPa) are estimated to be 3.5 × 10^{-19} and 1.3 × 10^{-18} $m^2 \cdot mol \cdot mol_{H2O}^{-1} \cdot s^{-1}$, respectively. Using these estimates of D^s_{N2} and D^s_{O2} at the two temperatures, Salamatin et al. [20] found the activation energy Q^s_m of the diffusive permeation.

Since X is proportional to pressure, D^s_m of m-molecule (i.e., N_2 or O_2) at the temperature T is given by

$$D^s{}_m = D^{s0}{}_m P^d{}_m \exp\left(-\frac{Q^s{}_m}{RT}\right), \tag{10}$$

where D^{s0}_m is a constant. Q^s_m is defined by the conventional relation:

$$D^s{}_m = D^s{}_m{}^* \frac{P^d{}_m}{P^d{}_m{}^*} \exp\left[\frac{Q^s{}_m}{R}\left(\frac{1}{T^*} - \frac{1}{T}\right)\right]. \tag{11}$$

Here, $D^s_m{}^*$ is the diffusive permeation coefficient at the reference temperature T^* and corresponding dissociation pressure $P^d_m{}^*$. Using Eq. (11), they roughly estimated

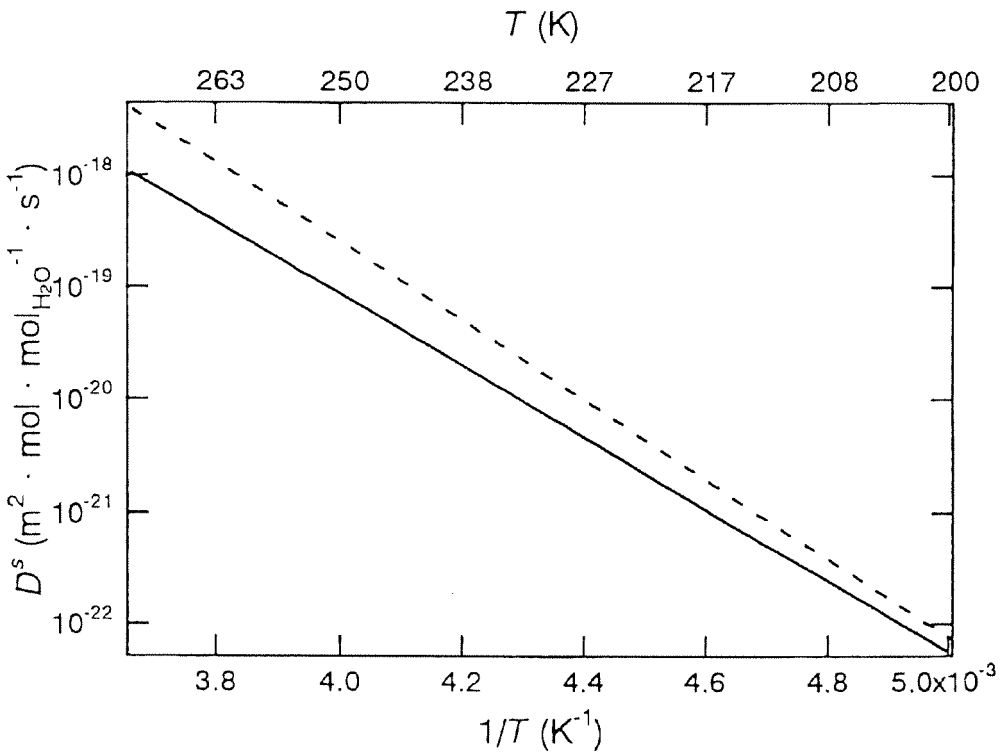

Figure 11: Temperature dependence of D^s_{N2} and D^s_{O2}. The solid and broken lines are D^s_{N2} and D^s_{O2}, respectively.

the common value of Q^s for N_2 and O_2 to be 50±3 kJ·mol^{-1} [20].

We attempt to estimate the temperature dependencies of D^s_{N2} and D^s_{O2} in order to apply the estimates to the conditions in polar ice sheets. Using Eq. (11), the separate values of Q^s_{N2} and Q^s_{O2} are estimated to be 48 and 54 kJ/mol, respectively. Substituting Eq. (2) into Eq. (10), we obtain $D^{s0}_{N2} = 1.1 \times 10^{-10}$ and $D^{s0}_{O2} = 7.8 \times 10^{-9}$ m^2·mol·mol$_{H2O}^{-1}$·s^{-1}·MPa^{-1}. Thus, D^s_{N2} and D^s_{O2} are calculated as shown in Fig. 11. From this figure, it can be seen that the D^s_{O2}/D^s_{N2} increases with increase in temperature. Therefore, it can be predicted that the effects of fractionation of gas molecules during the transition process from air-bubbles to clathrate hydrates essentially depend on the ice temperature in polar ice sheets.

5. Fractionation effects of gases in polar ice sheets

5.1. Vostok Antarctic ice

Using the approach described in the previous section, Salamatin et al. [20] simulated the variation of the N_2/O_2 ratio in a growing clathrate hydrate in the Vostok ice cores. They showed that the N_2/O_2 ratio of clathrate hydrate in the beginning of the transition zone decreases rapidly in comparison with the hydrate crystal growth, while those in the middle and the end of the transition zone remains practically constant during the transformation. They concluded that the gas composition in clathrate hydrates nucleated at the beginning of the transition zone completely vary due to the selective diffusion of O_2 during the period of their formation. On the other hand, the almost constant values of the N_2/O_2 ratio at the middle and the end of the transition zone were attributed to the following two reasons: (1) the radius of the initial air-bubble, r_{b0}, increases with increase in depth, and (2) the number of the surrounding air-bubbles decreases with increase in depth [45].

We attempt to apply the model [20] to the conditions of the Vostok ice, taking into account the above estimates of the temperature dependencies of D^s_{N2} and D^s_{O2}. The parameters at the beginning of the transition zone in the Vostok ice (600 m in depth) were assumed to be: $T = 220$ K (i.e., $P^d_{N2} = 3.6$ MPa, and $P^d_{O2} = 2.6$ MPa), $D^s_{N2} = 1.4 \times 10^{-21}$ m^2·mol·mol$_{H2O}^{-1}$·s^{-1}, $D^s_{O2} = 3.0 \times 10^{-21}$ m^2·mol·mol$_{H2O}^{-1}$·s^{-1}, $P_l = 5.1$ MPa, $n_b = 1$, $N_0 = 800$ cm^{-3}, and $\overline{Z}_{N_2} = 0.79$. Fig. 12 shows the simulated temporal variation of the N_2/O_2 ratio in a clathrate hydrate formed at a depth of 600 m. The difference between the two types A and B of the growth process can clearly be seen at the beginning. The inward growth of type B is rapid in comparison with that of type A, since the typical time of the compression of the air-bubble in the growth process of type B is one order of magnitude shorter than that in type A. On the other hand, the rate of the outward growth caused by the diffusive transfer of air molecules from the surrounding non-nucleated air-bubbles is approximately the same for both types. Therefore, at the beginning of the transition process, the N_2/O_2 ratio in the clathrate hydrate of type A decreases more rapidly in comparison with that of type B.

From Fig. 12, it can be seen that the rate of gas fractionation for both types A and B depends on r_{b0}. Because the number of clathrate hydrates is low in comparison with that of air-bubbles at the beginning of the transition zone, a considerable amount

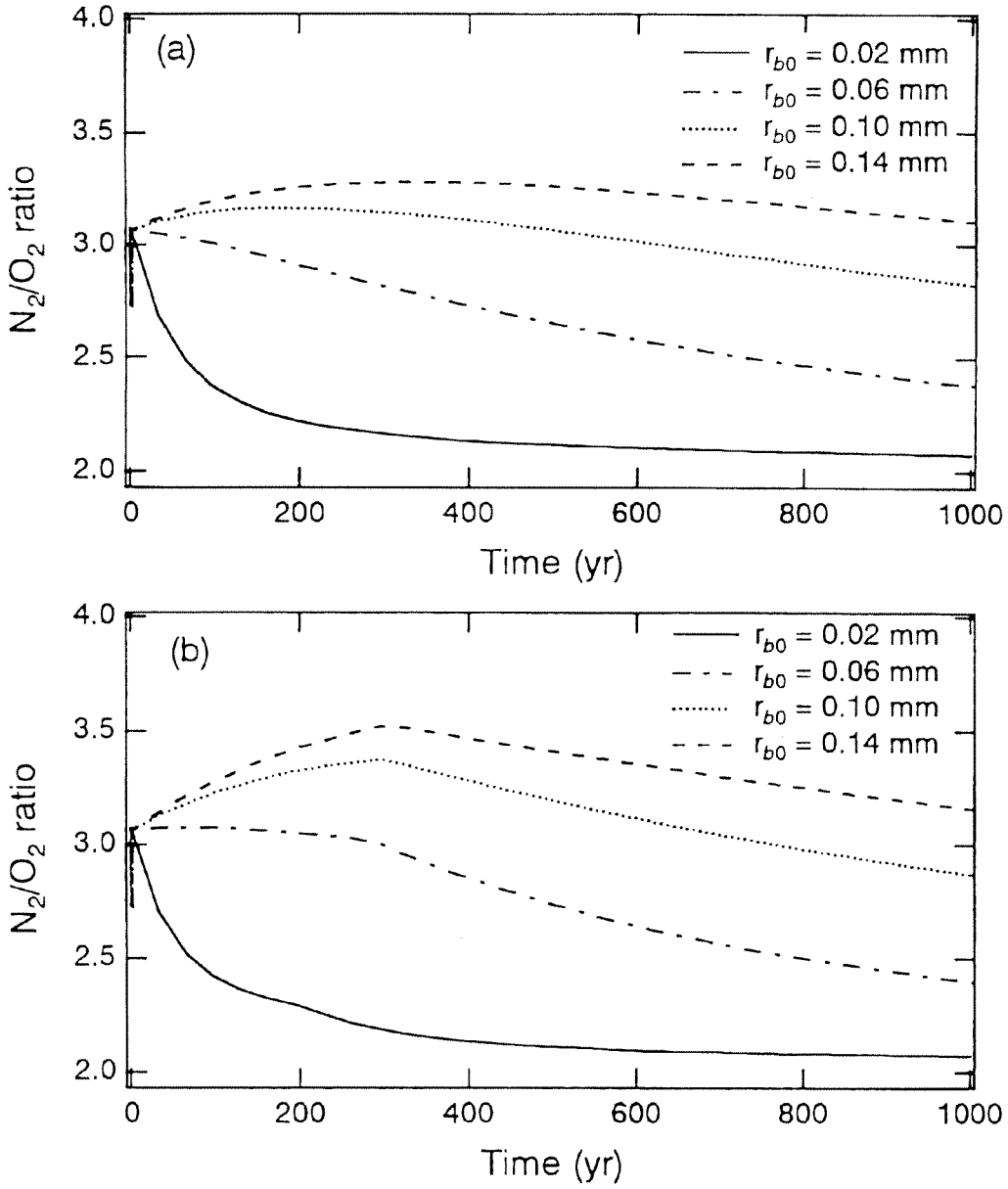

Figure 12: Temporal variation of the N_2/O_2 ratio in a clathrate hydrate at the beginning of the transition zone of the Vostok ice core (600 m in depth). (a) The growth process of type A. (b) The growth process of type B. r_{b0} is the radius of the initial air-bubble.

of air molecules is supplied to the clathrate hydrates from the surrounding non-nucleated air-bubbles. Thus, the N_2/O_2 ratio in all clathrate hydrates decreases rapidly, as shown by the solid lines in Fig. 12. Since the mass flux toward clathrate hydrates extracts O_2 preferentially from the surrounding non-nucleated air-bubbles, the N_2/O_2 ratios in the air-bubbles gradually increase. Accordingly, the N_2/O_2 ratios in

clathrate hydrates along the transition zone gradually increase, and they reach a value that is approximately equal to the atmospheric value at the end of the transition zone.

Fig. 13 (a) shows the simulated temporal variation of the N_2/O_2 ratio in a clathrate hydrate formed at the middle (800 m in depth) of the transition zone of the Vostok ice. The parameters at 800 m in

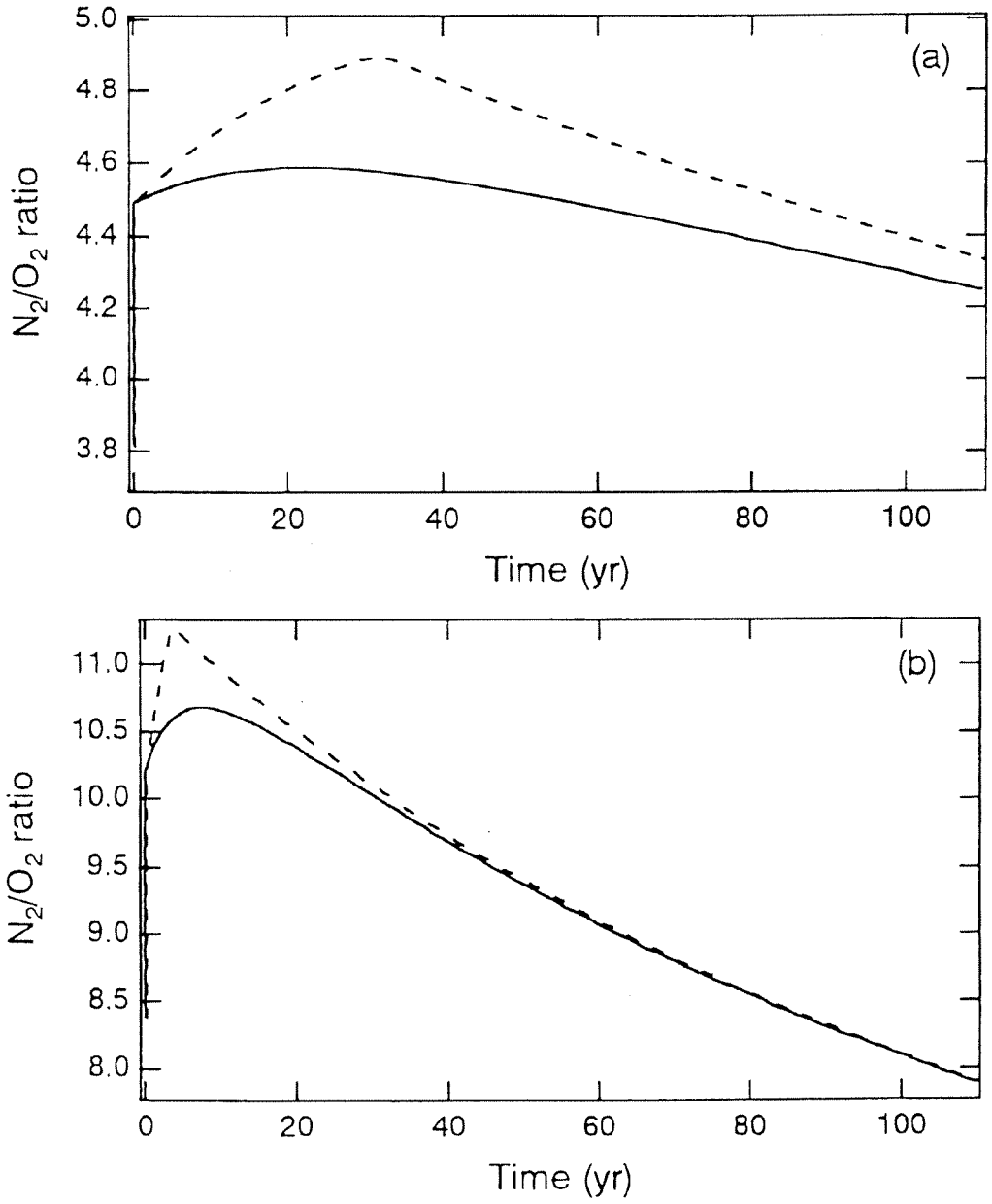

Figure 13: Temporal variation of the N_2/O_2 ratio in a clathrate hydrate at (a) the middle (800 m in depth), and (b) the end (1100 m in depth) of the transition zone of the Vostok ice. The solid and broken lines show the growth process of types A and B, respectively.

depth are assumed to be: T = 222 K (i.e., P^d_{N2} = 3.9 MPa, and P^d_{O2} = 2.8 MPa), D^s_{N2} = 1.9 × 10^{-21} $m^2 \cdot mol \cdot mol_{H2O}^{-1} \cdot s^{-1}$, D^s_{O2} = 4.2 × 10^{-21} $m^2 \cdot mol \cdot mol_{H2O}^{-1} \cdot s^{-1}$, P_l = 6.9 MPa, n_b = 0.45, N_0 = 800 cm^{-3}, $\overline{Z}_{N_2}$ = 0.84, $\overline{Y}_{N_2}$ = 0.75, and r_{b0} = 0.045 mm. From Fig. 12(a), it can be seen that the N_2/O_2 ratios of growing clathrate hydrates for both types A and B remain practically constant during the transformation.

Fig. 13 (b) shows the simulated temporal variation of the N_2/O_2 ratio in a clathrate hydrate formed at the end (1100 m in depth) of the transition zone of the Vostok ice [20]. The parameters at 1100 m in depth are assumed to be: T = 225 K (i.e., P^d_{N2} = 4.3 MPa, and P^d_{O2} = 3.1 MPa), D^s_{N2} = 3.0 × 10^{-21} $m^2 \cdot mol \cdot mol_{H2O}^{-1} \cdot s^{-1}$, D^s_{O2} = 6.9 × 10^{-21} $m^2 \cdot mol \cdot mol_{H2O}^{-1} \cdot s^{-1}$, P_l = 9.6 MPa, n_b = 0.05, N_0 = 800 cm^{-3}, $\overline{Z}_{N_2}$ = 0.92, $\overline{Y}_{N_2}$ = 0.79, and r_{b0} = 0.05 mm. The clathrate hydrate formed at the end of the transition zone initially has a very high N_2/O_2 ratio, because the N_2/O_2 ratio of the original air-bubble is very high. The N_2/O_2 ratio of the clathrate hydrate gradually decreases due to the diffusive air-mass exchange with the surrounding completely formed clathrate hydrates. In this case, the diffusive mass flux of air molecules between the clathrate hydrates is driven by the difference in the concentration of air molecules dissolved in the ice near the clathrate hydrates with different gas compositions.

If we assume that two clathrate hydrate crystals (crystal-*a* and crystal-*b*) with N_2/O_2 = 11.7 and 3.6 coexist in an ice core at 1100 m depth (i.e., at T = 225 K, P^d_{N2} = 4.3 MPa, and P^d_{O2} = 3.1 MPa), air molecules diffuse in the ice as follows. According to the assumption described in section 4.3, the values of X_{N2}^H and X_{O2}^H of ice at the interface with the crystal-*a* are 7.0 × 10^{-7} $mol \cdot mol_{H2O}^{-1}$ and 8.6 × 10^{-8} $mol \cdot mol_{H2O}^{-1}$, respectively. On the other hand, X_{N2}^H and X_{O2}^H of ice at the interface with the crystal-*b* are 5.6 × 10^{-7} $mol \cdot mol_{H2O}^{-1}$ and 2.3 × 10^{-7} $mol \cdot mol_{H2O}^{-1}$, respectively. Thus, O_2 molecules diffuse from the crystal-*b* toward the crystal-*a*, while N_2 molecules diffuse from crystal-*a* toward crystal-*b*. That is, O_2 and N_2 molecules diffuse through the ice in opposite directions. Because the number of newly formed clathrate hydrates is low in comparison with the number of completely formed clathrate hydrates at the end of the transition zone, the N_2/O_2 ratio of the clathrate hydrate with a very high N_2/O_2 ratio decreases rapidly. Accordingly, the N_2/O_2 ratios of clathrate hydrates are distributed around the original atmospheric value in the bubble-free ice zone.

5.2. Greenland ice

Using the model, Salamatin et al. [20] estimated that the gas-fractionation time scale in central Greenland is approximately comparable with that at Vostok, while the nucleation rate of clathrate hydrates in central Greenland is much (10 times) higher than that at Vostok. They concluded that significant gas fractionation, on average, is ruled out for clathrate hydrates in the Greenland ice cores.

Furthermore, we apply the model [20] to the conditions of the Greenland ice cores, taking into account the temperature dependencies of D^s_{N2} and D^s_{O2}. The transition zone in the GRIP ice is between 700 and 1300 m [14], which corresponds to a time period of about 4.5 kyr [34]. The ice temperature at the beginning of the transition zone (800 m, P_l = 7.2 MPa) of the GRIP ice is about 241 K [54]. Using Eq. (10), the values of D^s_{N2} and D^s_{O2} at 241 K (i.e., P^d_{N2} = 6.8 MPa, and P^d_{O2} = 5.1 MPa)

are estimated to be 2.6×10^{-20} and 7.7×10^{-20} $m^2 \cdot mol \cdot mol_{H2O}^{-1} \cdot s^{-1}$, respectively. The transition zone in the Dye-3 ice is between 1100 and 1650 m [41], which corresponds to a time period of about 4.1 kyr [33]. The temperature at the beginning of the transition zone (1100 m, P_l = 9.9 MPa) of the Dye-3 ice is about 254 K [41]. The values of D^s_{N2} and D^s_{O2} at 254 K (i.e., P^d_{N2} = 9.5 MPa, and P^d_{O2} = 7.2 MPa) are estimated as 1.3×10^{-19} and 4.3×10^{-19} $m^2 \cdot mol \cdot mol_{H2O}^{-1} \cdot s^{-1}$, respectively.

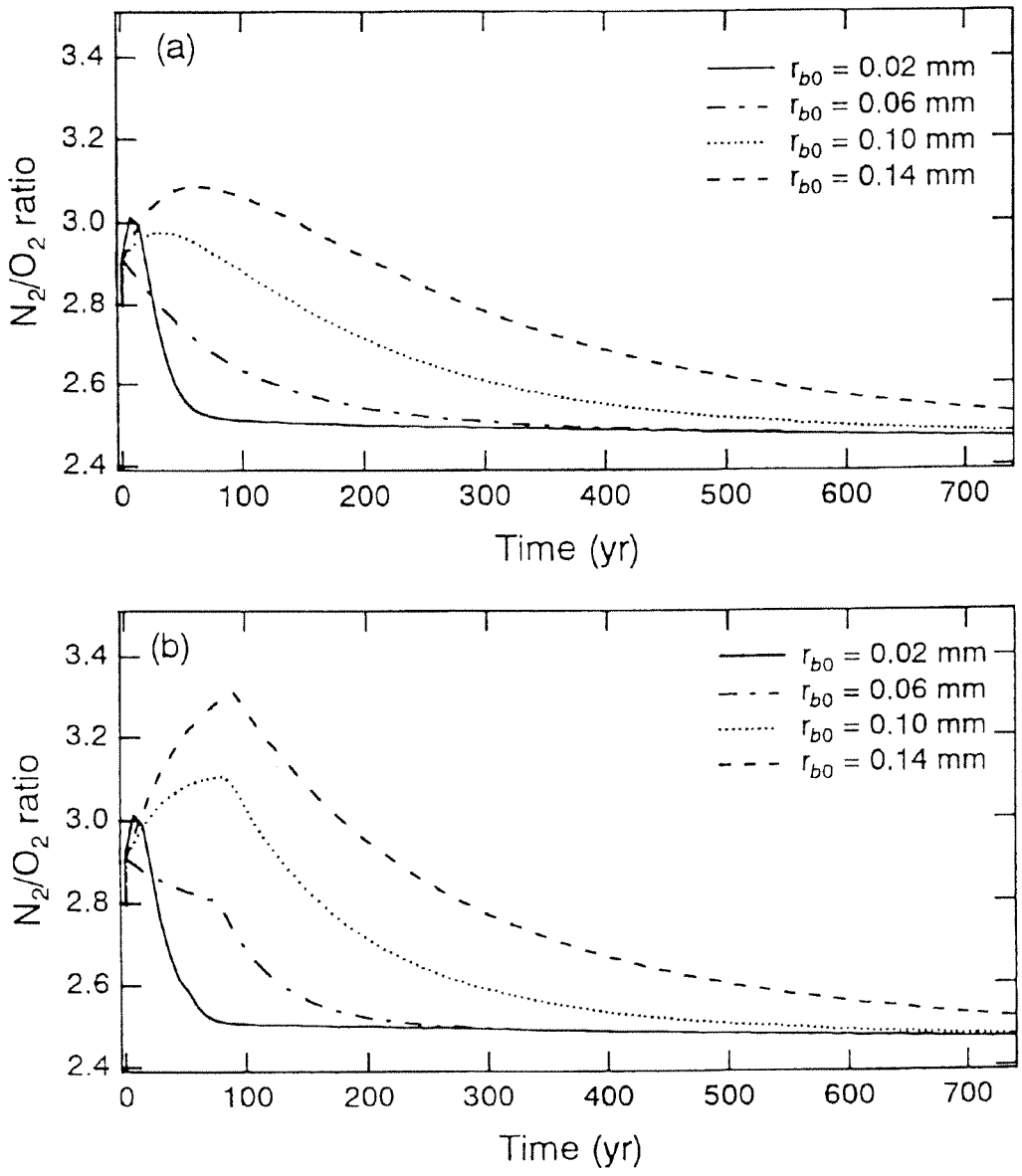

Figure 14: Temporal variation of the N_2/O_2 ratio in a clathrate hydrate at the beginning of the transition zone of the GRIP ice core (800 m in depth). (a) The growth process of type A. (b) The growth process of type B. r_{b0} is the radius of the initial air-bubble.

Under the assumptions of $n_b = 1$, $N_0 = 200$ cm^{-3}, and $\overline{Z}_{N_2} = 0.79$, the temporal variations of the N_2/O_2 ratio in a clathrate hydrate at the beginning of the transition zone in the GRIP and the Dye-3 ice cores are calculated, as shown in Figs. 14 and 15, respectively. From these figures, it can be seen that the N_2/O_2 ratios of the clathrate hydrates in both the GRIP and the Dye-3 ice cores decrease and approach certain values with time, although the nature of the variation depends on the value of r_{b0} and on

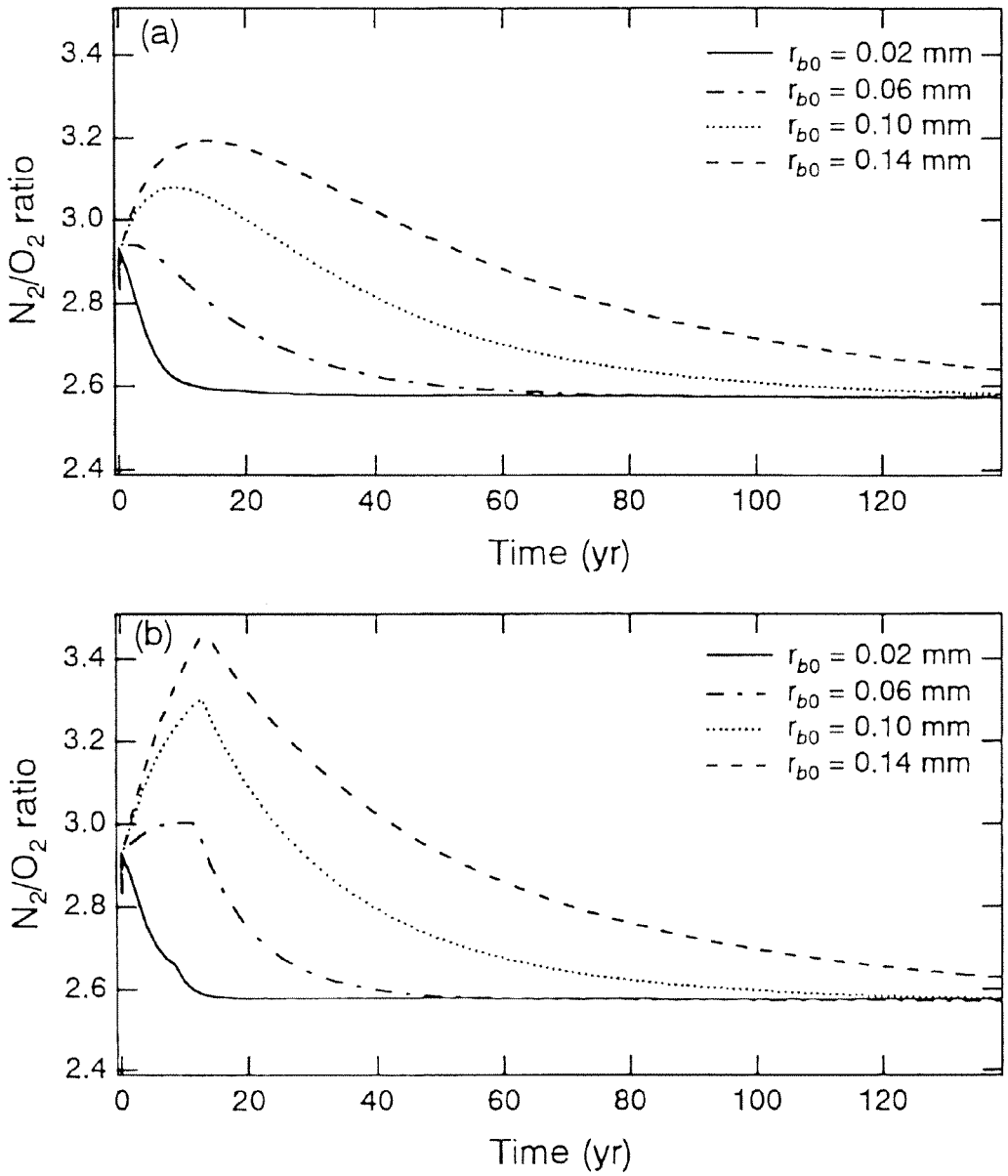

Figure 15: Temporal variation of the N_2/O_2 ratio in a clathrate hydrate at the beginning of the transition zone of the Dye-3 ice core (1100 m in depth). (a) The growth process of type A. (b) The growth process of type B. r_{b0} is the radius of the initial air-bubble.

the types of the growth process. The approached values are estimated using the following relation [20]:

$$\frac{D^s{}_{O_2}}{D^s{}_{N_2}} = \frac{M_{N_2}}{M_{O_2}} \left(\frac{P_l \overline{Z}_{N_2}}{P^d{}_{N_2} \overline{Y}_{N_2}} - 1 \right) \Bigg/ \left(\frac{P_l \overline{Z}_{O_2}}{P^d{}_{O_2} \overline{Y}_{O_2}} - 1 \right). \tag{12}$$

The composition of the surrounding non-nucleated air-bubbles (i.e., $\overline{Z}_{N_2} / \overline{Z}_{O_2}$) is about 3.7 at the beginning of the transition zone [19]. Therefore, using Eq. (12), the approached values (i.e., $\overline{Y}_{N_2} / \overline{Y}_{O_2}$) of the clathrate hydrates in the Vostok (600 m), GRIP (800 m), and Dye-3 (1100 m) ice cores are estimated as 2.1, 2.5, and 2.6, respectively.

The approached values of the clathrate hydrates in the GRIP and the Dye-3 ice cores are larger in comparison with that in the Vostok ice core. This is attributed to the temperature dependencies of the dissociation pressures of pure N_2- and O_2-clathrate hydrates. Since the dissociation pressures become closer (i.e., P^d_{N2}/P^d_{O2} approaches 1) with increases in temperature, the N_2/O_2 ratio of clathrate hydrate in ice at warmer condition approaches a higher value.

From Figs. 12, 14, and 15, it can be seen that the time scale of the variation of the N_2/O_2 ratio in the clathrate hydrate greatly depends on the ice temperature. Salamatin et al. [20] defined this time scale as the gas-mass exchange time scale τ_E. τ_E is given by

$$\tau_E \sim \frac{{r_{b0}}^2 P_{l0} P^d{}_{N_2}}{3 P_{iw} D^s{}_{N_2} \left[n_b \left(P_{l0} - P^d{}_{N_2} \right) + P^d{}_{N_2} \left| \overline{Z}_{N_2} - \overline{Y}_{N_2} \right| \right]}, \tag{13}$$

where P_{l0} is the initial pressure of the air-bubble, and P_{iw} is the apparent pressure at which the density of water molecules in the free gaseous phase are equal to that in ice [20].

Fig. 16 shows the relationship between r_{b0} and τ_E in the beginning of the transition zones of the Vostok (600 m), the GRIP (800 m), and the Dye-3 (1100 m) ice cores. The initial radius of air-bubbles in the ice sheet depends on the size of ice grains at the firn-ice transition (i.e., firn temperature and accumulation rate prevailing during ice formation). The value of r_{b0} in the beginning of the transition zones of the Vostok ice cores is about 0.02–0.06 mm [45], while that of the Greenland ice cores is about 0.1–0.15 mm [20]. From Fig. 16, it can be seen that the values of τ_E with r_{b0} = 0.1–0.15 mm in the Greenland ice cores are of approximately the same order as τ_E with r_{b0} = 0.02–0.06 mm in the Vostok ice cores.

The time periods of the transition zones in the Greenland ice are about one order of magnitude less than that in the Vostok ice, while the orders of τ_E are approximately equal. Thus, many other new clathrate hydrates with high N_2/O_2 ratios are nucleated during the gas-mass exchange time in the Greenland ice. Therefore, clear systematic variations in the averaged N_2/O_2 ratios in clathrate hydrates with depth were not found in the transition zone of the Greenland ice cores. At the end of the transition zone in the Greenland ice, the clathrate hydrate formed at the beginning of the transition zone has a low N_2/O_2 ratio, and the clathrate hydrate formed at the end of the transition zone has a high N_2/O_2 ratio. In other words, clathrate hydrates with a low N_2/O_2 ratio and those with a high N_2/O_2 ratio coexist at the same depth at the end of the transition zone in Greenland ice.

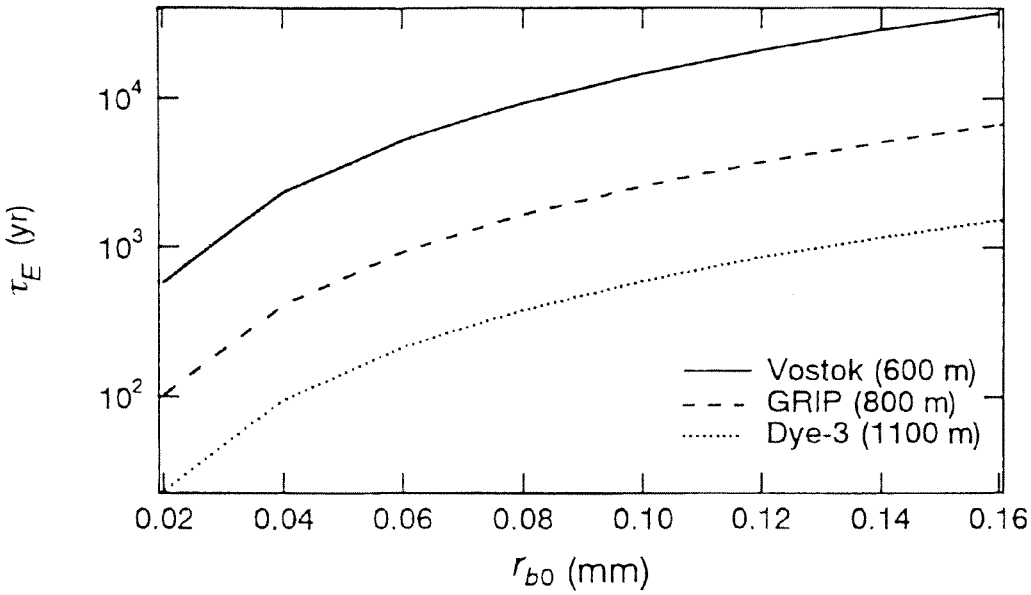

Figure 16: Relationship between the radius of the initial air-bubble r_{b0} and the time scale of the gas-mass exchange τ_E. The solid, broken, and dotted lines show τ_E in the beginning of the transition zones of the Vostok (600 m in depth), the GRIP (800 m in depth), and the Dye-3 (1100 m in depth) ice cores, respectively.

Actually, the N_2/O_2 ratios of clathrate hydrates were found to be distributed between 1.6 and 9.16 at a depth of 1501 m in the end of the transition zone in the Dye-3 ice core [11, 28]. The clathrate hydrate crystal with the N_2/O_2 ratio of 9.16 is thought to be formed at a deeper depth in the transition zone, because the crystal has clear facets and a remarkable non-uniform distribution of N_2/O_2 within the crystal [17, 28]. The growth of clathrate hydrate caused by the diffusion of air molecules from surrounding air-bubbles is comparatively slow at the end of the transition zone, since the number concentration of air-bubbles is much lower than that at the beginning of the transition zone. Thus, the newly formed crystal remains in the same state at the time of transformation from the air-bubble at the end of the transition zone. The N_2/O_2 ratios that are highly scattered at the end of the transition zone approach the original atmospheric value in the beginning of the bubble-free ice zone because of the diffusive mass transfer of air molecules between clathrate hydrates. Therefore, the distribution of N_2/O_2 ratios of clathrate hydrates in the GRIP ice cores (1219–2923 m) is small (i.e., 2.63–4.49) in comparison with that in Dye-3 ice cores [14, 15, 18].

Though a significant gas fractionation, on average, is ruled out for clathrate hydrates in the Greenland ice, the averaged N_2/O_2 ratios in the air-bubbles should increase with depth. The composition of air-bubbles (i.e., $\overline{Z}_{N_2}/\overline{Z}_{O_2}$) at the end of the transition zone is estimated using the following relation:

$$\frac{D^s_{O_2}}{D^s_{N_2}} = \frac{M_{N_2}}{M_{O_2}} \left(\frac{P_l}{P^d_{N_2}} - \frac{\overline{Y}_{N_2}}{\overline{Z}_{N_2}} \right) \Bigg/ \left(\frac{P_l}{P^d_{O_2}} - \frac{\overline{Y}_{O_2}}{\overline{Z}_{O_2}} \right), \quad (14)$$

which is an analogue of Eq. (12) [20]. The composition of surrounding completely formed clathrate hydrate (i.e., $\overline{Y}_{N_2}/\overline{Y}_{O_2}$) is about 3.7 at the end of the transition zone. Using Eq. (14), the values of $\overline{Z}_{N_2}/\overline{Z}_{O_2}$ of the air-bubbles in the Vostok (1100 m, T = 225 K), GRIP (1300 m, T = 240 K), and Dye-3 (1650 m, T = 256 K) ice cores are estimated as 11.2, 9.3, and 7.6, respectively. This agrees well with the direct measurements for the Vostok ice cores [19, 20]. Therefore, it is expected that the last air bubbles at the end of the transition zone in Greenland would also have the high N_2/O_2 ratios.

6. Conclusion

Significant fractionation of gas molecules in the transition zone was found from measurements of the depth profiles of N_2/O_2 composition ratios in clathrate hydrates and air-bubbles in the Vostok ice cores, using Raman spectroscopy [19]. In order to understand the fractionation process, a mathematical model of the post-nucleation growth of clathrate hydrate caused by the diffusive mass transfer of air molecules from air-bubbles through the surrounding ice matrix was developed [20]. The model was applied to the Greenland ice conditions. The calculations showed that there are no clear systematic variations in the average N_2/O_2 ratios in clathrate hydrates with depth in the transition zone of the Greenland ice. It was concluded that the effects of fractionation during the transition process of clathrate hydrates from air-bubbles on the distributions of air molecules are greatly dependent on the temperature in polar ice sheets.

The fractionation process of atmospheric gases in polar ice sheets demonstrates a valuable micro-physical process that cannot be observed on a laboratory time scale. The diffusion of monoatomic molecules and very small diatomic and polyatomic molecules such as H_2 and H_2O has been measured. However, the diffusion coefficients of N_2 and O_2 are too small to measure directly. It is possible to observe the diffusion phenomena of such large molecules as N_2 and O_2, because the polar ice sheets are maintained for a very long time.

The fractionation process should also be taken into account for a better understanding of the behavior of atmospheric gases (e.g., CO_2 and CH_4) other than N_2 and O_2 in polar ice sheets. Since diffusion occurs between air-bubbles and clathrate hydrates at distances in the order of 1 mm, no great correction may be required for current gas analysis of ice cores if a sufficiently large block of ice and appropriate extraction procedures are used. However, careful attention should be paid to the fractionation of atmospheric gases during the transition process from air-bubbles to clathrate hydrates in order to understand the rapid change in gas composition along the length of an ice core. The gas fractionation during the transition process from air-bubbles to clathrate hydrates might have important implications for the interpretation of gas distributions in ice sheets and the paleoatmospheric reconstruction.

Acknowledgments

We would like to thank Dr. B. Stauffer, Dr. W. F. Kuhs, Dr. H. Fukazawa, and Dr. P. Duval for their valuable discussion. This work was supported by a Grant-in-aid for Scientific Research from the Ministry of Science, Education and Sports, Japan. One of the authors, T. I., has been supported by a Research Fellowship of the Japan Society for the Promotion of Science for Young Scientists.

References

1. A. Neftel, E. Moor, H. Oeschger, and B. Stauffer, *Nature*, **315**, 45 (1985).
2. J.M. Barnola, D. Raynaud, Y.S. Korotkevich, and C. Lorius, *Nature*, **329**, 408 (1987).
3. D. Raynaud, J. Chappellaz, J.M. Barnola, Y.S. Korotkevich, and C. Lorius, *Nature*, **333**, 655 (1988).
4. A. Neftel, H. Oeschger, T. Staffelbach, and B. Stauffer, *Nature*, **331**, 609 (1988).
5. B. Stauffer, E. Lochbronner, H. Oeschger, and J. Schwander, *Nature*, **332**, 812 (1988).
6. D. Chappellaz, J.M. Barnola, D. Raynaud, Y.S. Korotkevich, and C. Lorius, *Nature*, **345**, 127 (1990).
7. S.L. Miller, *Science*, **165**, 489 (1969).
8. H. Shoji, and C.C. Langway, Jr., *Nature*, **298**, 548 (1982).
9. B. Stauffer, and J. Schwander, and H. Oeschger, *Ann. Glaciol.*, **6**, 108 (1985).
10. H. Graig, Y. Horibe, T. Sowers, *Science*, **242**, 1675 (1988).
11. J. Nakahara, Y. Shigesato, A. Higashi, T. Hondoh, and C.C. Langway, Jr., *Phil. Mag. B*, **57**, 421 (1988).
12. J. Schwander, J.M. Barnola, C. Andrie, M. Leuenberger, A. Ludin, D. Raynaud, and B. Stauffer, *J. Geophys. Res.*, **98**, 2831 (1993).
13. M. Bender, T. Sowers, and V.Ya. Lipenkov, *J. Geophys. Res.*, **100**, 18,651 (1995).
14. F. Pauer, J. Kipfstuhl, and W.F. Kuhs, *Geophys. Res. Lett.*, **22**, 969 (1995).
15. F. Pauer, J. Kipfstuhl, and W.F. Kuhs, *Geophys. Res. Lett.*, **23**, 177 (1996).
16. H. Fukazawa, T. Ikeda, T. Hondoh, P. Duval, V.Ya. Lipenkov, and S. Mae, *Proc. 2nd Int. Conf. on Natural Gas Hydrate*, p. 237 (1996).
17. H. Fukazawa, T. Ikeda, D. Suzuki, T. Hondoh, S. Mae, and C.C. Langway, Jr., in *Abst. Int. Symp. Physics and Chemistry of Ice* (Hanover, U.S.A., 1996), p. 120.
18. F. Pauer, J. Kipfstuhl, and W.F. Kuhs, *J. Geophys. Res.*, **102**, 26,519 (1997).
19. T. Ikeda, H. Fukazawa, S. Mae, L. Pepin, P. Duval, B. Champagnon, V.Ya. Lipenkov, and T. Hondoh, *Geophys. Res. Lett.*, **26**, 91 (1999).
20. A.N. Salamatin, T. Hondoh, V.Ya. Lipenkov, and T. Ikeda, *Ann. Glaciol.*, (in press).
21. T. Blunier, J. Schwander, and B. Stauffer, in *Physics of Ice-Core Records*, edited by T. Hondoh, (Hokkaido Univ. Press, Sapporo, 2000), (in press).
22. M. von Stackelberg, and H.R. Muller, *Z. Elektrochem*, **58**, 25 (1954).
23. R.K. McMullen and G.A. Jeffrey, *J. Chem. Phys.* **42**, 2725 (1965).
24. T.C. Mak and R.K. McMullen, *J. Chem. Phys.* **42**, 2732 (1965).
24. D.W. Davidson, Y.P. Handa, C.I. Ratcliffe, and J.S. Tse, *Nature*, **311**, 142 (1984).

26. D.W. Davidson, S.R. Gough, Y.P. Handa, C.I. Ratcliffe, J.A. Ripmeester, and J.S. Tse, *J. Phisique*, **48**, CI-537 (1987).
27. T. Hondoh, H. Anzai, A. Goto, S. Mae, A. Higashi, and C.C. Langway, Jr., *J. Incl. Phenom. Recogn. Chem.*, **8**, 17 (1990).
28. T. Ikeda, H. Fukazawa, S. Mae, T. Hondoh, and C.C. Langway, Jr., *J. Phys. Chem.*, **101**, 6180 (1997).
29. W. F. Kuhs, B. Chazallon, P.G. Radaelli, and F. Pauer, *J. Incl. Phenom. Recogn. Chem.*, **29**, 65 (1997).
30. A.N. Salamatin, T. Hondoh, T. Uchida, and V.Ya. Lipenkov, *J. Cryst. Growth*, **193**, 197 (1998).
31. V.Ya. Lipenkov, *Mater. Glyatsiol. Issled.*, **65**, 58 (1989).
32. T. Uchida, P. Duval., V.Ya. Lipenkov, T. Hondoh, S. Mae, and H. Shoji, *Mem. Natl. Inst. Polar Res., Spec. Issue*, **49**, 298 (1994).
33. C.U. Hammer, in Environmental Record in *Glaciers and Ice Sheets*, edited by H. Oeschger, and C. C. Langway, Jr., (Wiley, New York, 1989) p. 99.
34. W. Dansgaard, S.J. Johnsen, H.B. Clausen, D. Dahl-Jensen, N.S. Gundestrup, C.H. Hammer, C.S. Hvidberg, J.P. Steffensen, A.E. Sveinbjornsdottir, J. Jouzel, and G. Bond, *Nature*, **364**, 218, (1993).
35. T. Uchida, T. Hondoh, S. Mae, P. Duval, and V.Ya. Lipenkov, in *Physics and Chemistry of Ice*, edited by N. Maeno and T. Hondoh, (Hokkaido Univ. Press., Sapporo, 1992), p. 121.
36. T. Uchida, T. Hondoh, S. Mae, P. Duval, and V.Ya. Lipenkov, *Ann. Glaciol.*, **20**, 143 (1994).
37. K. Goto, T. Hondoh, and A. Higashi, *Jpn. J. Appl. Phys.*, **25**, 351 (1986).
38. P.B. Price, *Science*, **267**, 1802 (1995).
39. A.J. Gow, and T. Williamson, *J. Geophys. Res.*, **80**, 5101 (1975).
40. N.I. Barkov, and V.Ya. Lipenkov, *Mater. Glyatsiol. Issled.*, **51**, 178 (1984).
41. T. Hondoh, in *Proc. 2nd Int. Conf. Natural Gas Hydrate*, p. 131 (1996).
42. R.M. Barrer, and W.I. Stuart, *Proc. Roy. Sci. London*, **243**, 172 (1958).
43. D.W. Davidson, in *Water– A Comprehensive Treatise*, edited by F. Franks, (Plenum Press, New York, 1972), Vol. 2, Chap. 3.
44. M. von Stackelberg, *Naturwissenschaften*, **36**, 327, 359, (1949).
45. V.Ya. Lipenkov, in *Physics of Ice-Core Records*, edited by T. Hondoh, (Hokkaido Univ. Press, Sapporo, 2000), (in press).
46. J.H. van der Waals, and J.C. Platteeuw, *Adv. Chem. Phys.*, **2**, 1, (1959).
47. V.Ya. Lipenkov and A.N. Salamatin, *Antarktika* (Doklady Komissii), **28**, 59 (1989).
48. K. Satoh, T. Uchida, T. Hondoh, and S. Mae, *Proc. NIPR Symp. Polar Meteorol. Glaciol.*, **10**, 73, (1996).
49. J.P. Bouanich, *J. Quant. Spectrosc. Radiat. Transfer*, **47**, 243, (1992).
50. Kittel, in *Introduction to Solid State Physics, 7th ed.*, (John Wiley and Sons Inc., New York, 1972) p. 60.
51. H. Itoh, K. Kawamura, T. Hondoh, and S. Mae, *J. Chem. Phys.*, **105**, 2408, (1996).
52. C. Mellot, and J. Lignieres, *Molec. Simulation*, **18**, 349, (1997).
53. H.L. Strauss, Z. Chen, and C.K. Loong, *J. Chem. Phys.*, **101**, 7,177, (1994).
54. N.S. Gundestrup, D. Dahl-Jensen, S.J. Johnsen, and A. Rossi, *Cold Regions Science Technology*, **21**, 399, (1993).